



# LUND UNIVERSITY

## Structure and dynamics of complex materials in the water-poor regime

Gustavsson, Sanna

2016

[Link to publication](#)

*Citation for published version (APA):*

Gustavsson, S. (2016). *Structure and dynamics of complex materials in the water-poor regime*. [Doctoral Thesis (compilation), Physical Chemistry]. Lund University, Faculty of Science, Department of Chemistry, Division of Physical Chemistry.

*Total number of authors:*

1

### General rights

Unless other specific re-use rights are stated the following general rights apply:

Copyright and moral rights for the publications made accessible in the public portal are retained by the authors and/or other copyright owners and it is a condition of accessing publications that users recognise and abide by the legal requirements associated with these rights.

- Users may download and print one copy of any publication from the public portal for the purpose of private study or research.
- You may not further distribute the material or use it for any profit-making activity or commercial gain
- You may freely distribute the URL identifying the publication in the public portal

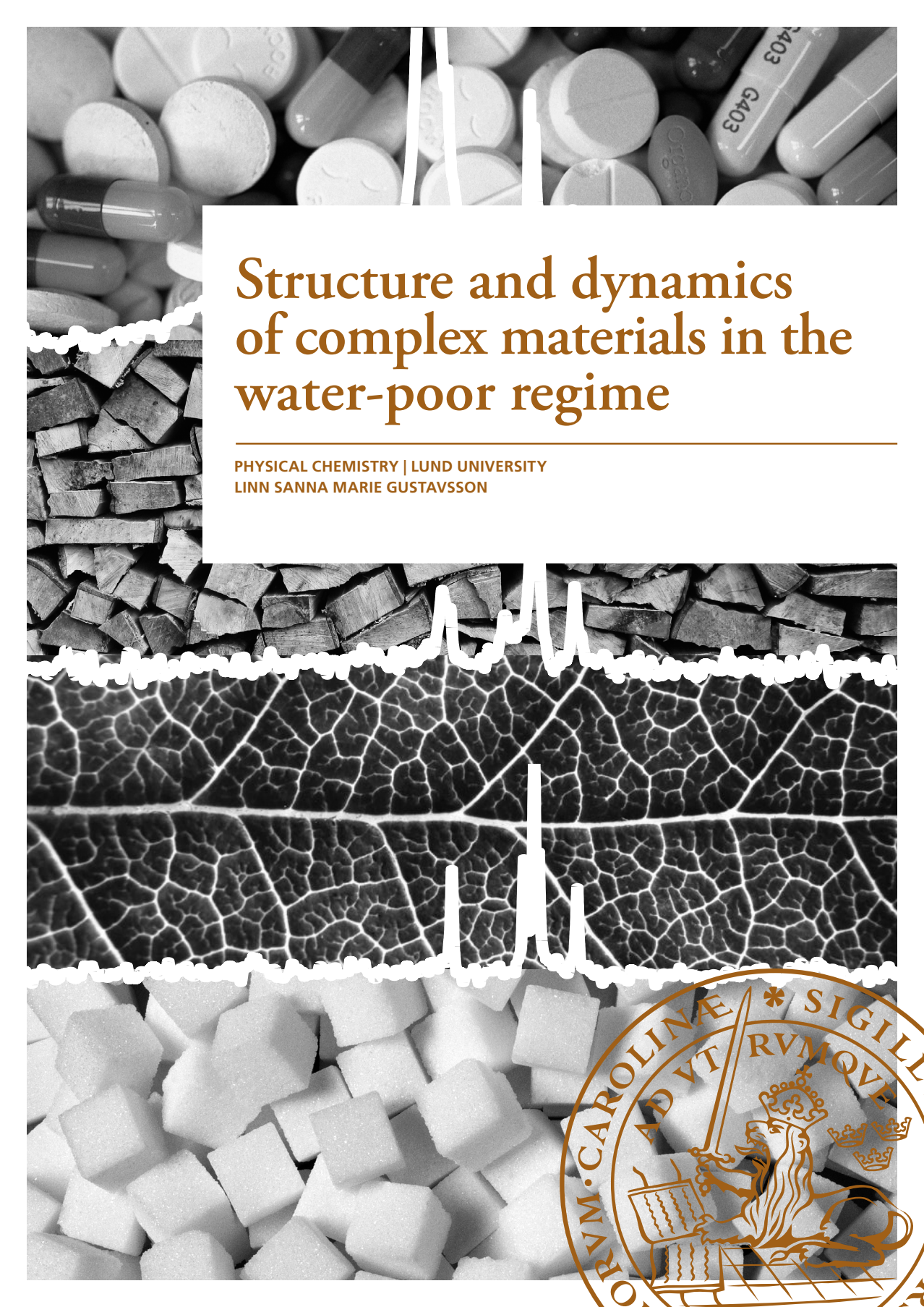
Read more about Creative commons licenses: <https://creativecommons.org/licenses/>

### Take down policy

If you believe that this document breaches copyright please contact us providing details, and we will remove access to the work immediately and investigate your claim.

LUND UNIVERSITY

PO Box 117  
221 00 Lund  
+46 46-222 00 00

The background is a collage of three distinct textures: the top section shows various pills and capsules, the middle section shows a pile of wood chips, and the bottom section shows white sugar cubes. A white ECG line is overlaid on the collage, with its peaks and troughs corresponding to the boundaries between the different textures.

# Structure and dynamics of complex materials in the water-poor regime

---

PHYSICAL CHEMISTRY | LUND UNIVERSITY  
LINN SANNA MARIE GUSTAVSSON





# Structure and dynamics of complex materials in the water-poor regime

Linn Sanna Marie Gustavsson  
Division of Physical Chemistry  
Lund University, Sweden



**LUND**  
UNIVERSITY

Thesis for the Degree of Doctor of Philosophy in Physical Chemistry

To be presented, with the permission of the Faculty of Science of Lund University, for public criticism in  
the lecture hall B at the Center for Chemistry and Chemical Engineering (Kemicentrum),  
Naturvetarvägen 14, 221 00 Lund, on Friday 10 June 2016, 09:00.

*Faculty opponent*  
Prof. Sven Engström  
Chalmers University of Technology, Gothenburg, Sweden

Organization <b>LUND UNIVERSITY</b> Division of Physical Chemistry P.O. Box 124 SE-221 00 LUND Sweden		Document name <b>DOCTORAL DISSERTATION</b>	
		Date of issue 2016-06-10	
Author(s) Linn Sanna Marie Gustavsson		Sponsoring organization	
Title and subtitle Structure and dynamics of complex materials in the water-poor regime			
Abstract <p>In the solid state, molecules are normally ordered in a specific structure. With time, and as a result of influence from the surroundings, solid materials can change their molecular and/or crystal structure and, as a consequence, obtain completely different properties. Water is particularly important in this respect. Adsorption of minuscule amounts of water from the atmosphere may have huge effects on the properties and stability of solid materials. For instance, in pharmaceuticals this can lead to harmful consequences if an active substance, with a specific solid-state structure, suddenly changes due to interaction with adsorbed moisture. In processing and during storage, it is therefore important to have a detailed molecular understanding of the material properties and how they depend on water content. The primary aim of this thesis is to investigate the effects of small amounts of adsorbed water on molecular structure and dynamics in complex materials. In this water-poor regime (loosely defined as &lt;5% of water), solid substances are normally investigated by means of X-ray scattering, gravimetric techniques and calorimetry. In the thesis, these conventional techniques are supplemented by solid-state NMR. This opens new possibilities to understand not only the structure, but also the dynamics of the materials. The complex materials investigated in the thesis belong to the two large substance classes of surfactants and polymers. These types of substances are used widely in everyday products, such as pharmaceuticals, paper, textiles, cosmetics and hygiene products. The results in the thesis show that solid-state NMR can be used to construct the equilibrium phase diagram of surfactant systems, in this case tetradecylmaltoside/H<sub>2</sub>O in the water-poor regime, and also to determine the regions of metastability of the non-equilibrium solid phases. The combination of solid-state NMR and X-ray scattering is a powerful tool to elucidate the structure and molecular dynamics of crystalline carbohydrates, exemplified by cyclodextrins, upon hydration. Similarly, solid-state NMR was used to extract information about molecular structure and dynamics in different stages of cellulose dissolution. The solid and dissolved cellulose was investigated in aqueous dissolution media together with cosolutes sodium hydroxide or tetrabutylammonium hydroxide. Another area of application of polymers is within renewable power energy where they are used in polymer electrolyte membrane fuel cells. As a way of optimizing the functionality we used NMR-based diffusometry to investigate transport behaviour as a function of polymer membrane structure, temperature and water content.</p>			
Key words hydration, cellulose, dissolution, sugar surfactant, hydrated crystals, structure, dynamics, phase diagram, fuel cell, pulsed-field-gradient stimulated spin-echo (PFG) NMR, Polarization Transfer solid state NMR, PXRD, GVS, TGA, amphiphilic			
Classification system and/or index terms (if any)			
Supplementary bibliographical information		Language English	
ISSN and key title		ISBN 978-91-7422-449-8	
Recipient's notes		Number of pages 94	Price
		Security classification	

I, the undersigned, being the copyright owner of the abstract of the above-mentioned dissertation, hereby grant to all reference sources the permission to publish and disseminate the abstract of the above-mentioned dissertation.

Signature \_\_\_\_\_

Date 2016-04-29 \_\_\_\_\_

# Structure and dynamics of complex materials in the water-poor regime

Linn Sanna Marie Gustavsson



**LUND**  
UNIVERSITY

**Funding information:** The thesis work was financially supported by Crafoord Foundation and Swedish Research Council (grant nos. 2009-6794 and 2011-4334).

© Linn Sanna Marie Gustavsson 2016

Faculty of Science, Division of Physical Chemistry, Lund University  
ISBN: 978-91-7422-449-8 (print)

Printed in Sweden by Media-Tryck, Lund University, Lund 2016



*Dedicated to my family*



# Contents

List of publications . . . . .	ii
Author contributions . . . . .	iii
Popular summary . . . . .	iv
Populärvetenskaplig sammanfattning . . . . .	v
<b>Structure and dynamics of complex materials in the water-poor regime</b>	<b>1</b>
1 Introduction . . . . .	1
1.1 Sugar surfactants . . . . .	3
1.2 Cyclodextrins . . . . .	5
1.3 Cellulose . . . . .	8
1.4 Polymer electrolyte membranes . . . . .	10
2 Experimental methodology . . . . .	12
2.1 Sample preparation . . . . .	12
2.2 Nuclear Magnetic Resonance (NMR) . . . . .	12
2.3 Powder X-ray diffraction (PXRD) . . . . .	16
2.4 Dynamic Sorption Balance . . . . .	17
2.5 Thermogravimetric Analysis . . . . .	17
3 Main results of the research papers . . . . .	18
4 Conclusions . . . . .	39
5 Acknowledgements . . . . .	40
6 References . . . . .	41
<b>Scientific publications</b>	<b>47</b>
Paper I: Equilibrium and non-equilibrium phases of alkylglycoside <i>n</i> -tetradecyl- $\beta$ -D-maltoside in the water-poor regime . . . . .	49
Paper II: Effect of Water Activity on the Structure, Dynamics and Hydration of Crystalline $\alpha$ -, $\beta$ -, and $\gamma$ -Cyclodextrin . . . . .	59
Paper III: Polarization transfer solid-state NMR: a new method for studying cellulose dissolution . . . . .	69
Paper IV: Structure-Property Correlations of Ion-Containing Polymers for Fuel Cell Applications . . . . .	75

## List of publications

This thesis is based on the following publications, referred to by their Roman numerals:

- I **Equilibrium and non-equilibrium phases of alkylglycoside *n*-tetradecyl- $\beta$ -D-maltoside in the water-poor regime**  
S. Gustavsson, J. Algotsson, A. Nowacka, J. Reimer, S. Ulvenlund, D. Topgaard  
Manuscript, 2016
- II **Effect of Water Activity on the Structure, Dynamics and Hydration of Crystalline  $\alpha$ -,  $\beta$ -, and  $\gamma$ -Cyclodextrin**  
S. Gustavsson, J. Reimer, O. Söderman, S. Ulvenlund  
Manuscript, 2016
- III **Polarization transfer solid-state NMR: a new method for studying cellulose dissolution**  
S. Gustavsson, L. Alves, B. Lindman, D. Topgaard  
RSC Adv., 2014, 4, 31836–31839
- IV **Structure-Property Correlations of Ion-Containing Polymers for Fuel Cell Applications**  
V. Sproll, G. Nagy, U. Gasser, S. Balog, S. Gustavsson, T.J. Schmidt, L. Gubler  
Radiat. Phys. Chem, 2016, 118, 120–123

All papers are reproduced with permission of their respective publishers.

## **Author contributions**

- I Responsible for some of the experimental work and NMR-experiments, and the major part of the writing.
- II Responsible for all the experimental work, and a part of the writing.
- III Responsible for NMR-experiments and analysis, and parts of the writing.
- IV Responsible for some of the experimental work and all of the NMR-experiments, and a small part of the writing.

## Popular summary

Carbohydrate systems like alkylpolyglycoside (APGs) surfactants, cellulose, and cyclodextrin are environmentally friendly renewable materials that are used widely in our daily life; as drug carriers for active substances in the pharmaceutical industry, as dietary fibre in the food industry, in paper, in cosmetics and hygiene products to name a few. They are solid substances built up of molecules ordered in a specific structure. With time, and potential influence from the surroundings, such as water vapour and temperature, these materials can change their molecular and/or crystal structure and obtain completely different properties. The smallest sorption of water from the atmosphere may have large effects on the functionality and stability. For instance, in pharmaceuticals this can lead to detrimental consequences if an active substance, with a specific molecular structure and functionality, suddenly changes its structure. The properties of the new material might be harmful instead. In processing and during storage it is important to have a detailed molecular knowledge of the properties of how a substance reacts to outer influence. Usually these "almost" dry substances are characterized by light scattering techniques, gravimetric techniques (weighing) and calorimetry (heat-change). Nuclear Magnetic Resonance (NMR) has lately been proven useful when investigating solid and semi-solid (liquid crystalline) materials. In this way one can systematically investigate material properties such as structure and dynamics for a specific segment in a molecule as a function of water content and temperature. It is also important for optimization of the production and to keep economic costs low. Polymers are widely used in today's society. One of those areas is renewable power energy where they are used in fuel cells. Fuel cells are similar to a battery, but without the need for replacement or recharge, as long as oxygen and hydrogen is provided. The benefit to the environment is that fuel cells have no combustion. However, the manufacturing of the hydrogen fuel is not without pollution. As a way of optimizing the functionality NMR diffusometry is used to investigate transport behaviour as a function of polymer membrane structure as a function of temperature and water content.

## Populärvetenskaplig sammanfattning

Kolhydratsystem så som alkylglycosider, cellulosa och cyklodextrin är miljövänliga förnybara material som används inom många områden i dagens samhälle; som bärare av aktiva substanser i läkemedelstabletter, matsmältningsfiber, papper, kosmetika och hygienartiklar för att nämna några. De är fasta substanser uppbyggda av molekyler ordnade i en viss struktur. Med tiden, och eventuell yttre påverkan, som t ex. vattenupptag och temperaturförändringar, så kan dessa material ändra sin uppbyggnad och då få helt andra egenskaper. Små upptag av vatten från atmosfären kan leda till stora ändringar i funktionalitet och hållbarhet. Det är därför viktigt att ha detaljerad kunskap om hur molekylstrukturen påverkar dynamiken och stabiliteten samt funktionaliteten av en substans. Vanligtvis så karakteriserer man denna typ av torrasystem med ljus-spridningsteknik (röntgen), gravimetriska tekniker (vägning) och kalorimetri (värmemängdsmätning). Kärnmagnetresonans (NMR) har på senare tid visat sig användbart när man studerar fasta material såväl som halvfasta (flytande kristallina) material. Med denna teknik kan man systematisk undersöka materialegenskaper i form av struktur och dynamik i specifika segment i molekylen som funktion av vattenhalt och temperatur. Det är även viktigt för att optimisera tillverkningsprocessen samt hålla ekonomiska kostnader nere. Polymerer används flitigt i dagens samhälle. Ett av de områdena är inom förnybar energi där man använder dem i bränsleceller. Bränsleceller är som ett batteri. De är uppbyggda av ett elektriskt ledande material som är placerat mellan två elektroder. Till skillnad från batterier så kräver bränsleceller ingen uppladdning eller något byte. De drivs så länge bränsle och oxidationsmedel tillförs (vanligen syre och väte) utifrån till elektroderna. Fördelen för miljön är att bränsleceller inte har någon förbränning. Däremot så är framställningen av bränslet (väte) inte föroreningsfri. Vi undersöker hur transporten av vatten relaterar till strukturen av polymer membranet och dess egenskaper. Eftersom vatten transporten är viktig för en bränslecells funktionalitet så undersöker vi även diffusionen vid olika vattenhalter och temperaturer för att kunna optimera bränslecellens egenskaper.



# Structure and dynamics of complex materials in the water-poor regime

## 1 Introduction

In our everyday life we use surfactants and polymers, because of their wide range of properties, in applications such as pharmaceuticals, textiles, detergents, foods, cosmetics, hygienic products, fuel cells, the list goes on. Surfactants are amphiphilic molecules built up of a hydrophilic (water-loving/ polar) head group and a hydrophobic (water-hating/ nonpolar) tail. The head group can be of different origin but the tail is usually a hydrocarbon chain of two or more carbon segments. Polymers are large molecules built up of smaller molecules or subunits called monomers. Like surfactants, many polymers are also amphiphilic depending on molecular conformation. Both surfactants and polymers can form a wide range of crystal structures, semi-crystalline structures and glass structures with unique physical properties.

Since these solid, and semi-solid materials are used in different applications, for their specific functions, it is crucial to have a detailed understanding of the materials properties to ensure correct functionality. When working with solid systems it is important to realise that sorption of atmospheric water might have a pronounced effect on a materials functionality, as well as physical and chemical stability, due to the structural changes and chemical reactions it can cause. Therefore it is crucial to know where the water ends up in the solid structure and what effects it has. This is important not only during processing, usage, and storage but also for optimizing material properties and development of new materials with properties designed for specific applications. A good approach to get an overview of how microscopic properties relate to the macroscopic properties is to construct phase diagrams. Phase diagrams visualize the borders between the equilibrium solid, semi-solid and liquid phases. This thesis focuses on carbohydrate systems because they are so called green chemicals, have a wide range of applications, and have very rich phase behaviours due to their amphiphilic nature.

The first part of this thesis gives an introduction to carbohydrate systems investigated in this thesis followed by a description of the techniques that were used. The second part is a summary of the different studies.

In paper I and II concerns carbohydrate systems investigated in the “almost dry” regime, with up to 10 wt% water concentration, as a function of water content and temperature by combining Polarization Transfer solid-state NMR, Powder X-ray Diffraction and gravimetric techniques. Paper I is a study on the phase structures and molecular dynamics of the alkylglycoside n-tetradecyl- $\beta$ -D-maltoside ( $C_{14}G_2$ ) at different relative humidities and temperatures. A phase diagram of  $C_{14}G_2/H_2O$  in the water-poor regime is presented in paper II. The structure and molecular dynamics of  $\alpha$ -,  $\beta$ - and  $\gamma$ -cyclodextrins are investigated upon stepwise increasing hydration and temperature, as well as their influence on the packing motifs.

Paper III is an illustration on the power of the polarization transfer solid-state NMR technique to give molecular-level information on dissolved and solid cellulose in aqueous dissolution media with sodium hydroxide or tetrabutylammonium hydroxide.

Paper IV present a structure–property correlations study of grafted proton conducting membranes used in fuel cells. Pulse Field Gradient diffusion NMR was used to address functional changes of a polymer membranes upon grafting level, hydration level, and temperature.

## 1.1 Sugar surfactants

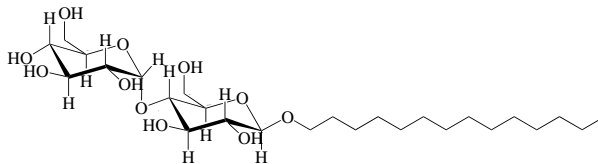


Figure 1: Molecular structure of *n*-tetradecyl- $\beta$ -D-maltoside  $\beta$ -C<sub>14</sub>G<sub>2</sub>.

Alkylglycosides are non-ionic sugar surfactants which consist of a hydrophilic head-group with one or more sugar units and a hydrophobic alkyl chain. They can be synthesised from naturally occurring renewable resources, fatty alcohols and sugars, usually glucose or maltose. They are biodegradable, with low-toxicity and have a unique physiochemical behaviour. They have been extensively used in industrial applications such as cosmetics, detergents, emulsifiers, wetting and solubilizers.[1–4] The head-groups of alkylglycosides consist of several hydroxyl groups. They can interact strongly with neighbouring groups through intermolecular hydrogen bonds, leading to the formation of a wide range of possible configurations and hence to a very interesting solid phase behaviour. Fischer et al[5] have previously reported on the two-step melting of glucose surfactant systems. The first of these "double melting points" is called the "chain melting" and the second is called the "clearing point". At the "chain melting" point the energy of the thermal motion overpowers the van der Waals forces between the alkyl chains and this leads to an order-disorder transition and the formation of the a liquid crystalline phase. There is still long-range orientational ordering in the structure due to the interaction of the head groups. However, the translational order varies. Due to the amphiphilic nature of the alkylglycosides, they usually form lamellar crystalline phases. At the second melting point, the "clearing point", the structure collapses and an isotropic liquid is formed. At this temperature not even the strong interactions in the head-groups can withstand the thermal motion. Jeffrey et al[6] showed that the "clearing point" is dependent on the ability to form hydrogen bonds in the head-groups. Alkylmaltosides have a larger gap between the "chain melting" and the "clearing point" than the alkylglucosides.

The alkylmaltoside *n*-dodecyl- $\beta$ -D-maltoside ( $\beta$ -C<sub>12</sub>G<sub>2</sub>), has been extensively studied. [7] Surfactants with even longer alkyl chains are useful in, e.g. micellar solubilisation of bulky organic molecules.[8] They are also good model systems for investigations with respect to water sorption and water interactions as an aid in understanding more complicated systems where oligo- and polysaccharide chains play an important role in structure, e.g., cellulose, glycolipids, and glycoproteins.

Ericsson et al[8] have investigated the thermotropic phase behaviour of  $\beta$ -C<sub>14</sub>G<sub>2</sub>. They found that the solid phase behaviour has a strong dependence on kinetics. An unusual feature of surfactant systems like  $\beta$ -C<sub>14</sub>G<sub>2</sub> (and  $\beta$ -C<sub>8</sub>G<sub>2</sub>) is that at low water content it undergoes glass transitions.[8–10] Ericsson et al[8] reported that  $\beta$ -C<sub>14</sub>G<sub>2</sub> is in an anhydrous, lamellar liquid crystalline phase at temperatures above 105°C. At temperatures below 105°C the  $\beta$ -C<sub>14</sub>G<sub>2</sub> was reported to form no less than five different solid phases, depending on kinetics. More specifically, the different phases are two different anhydrous, non-crystalline states that differ by the ordering of the head-groups and at least two different anhydrous crystalline polymorphs, which differ by the tilt angle of the alkyl chains. In addition,  $\beta$ -C<sub>14</sub>G<sub>2</sub> also form a crystalline hemihydrate. Ericsson et al[8] have also proposed structures for the ( $\beta$ -C<sub>14</sub>G<sub>2</sub>) which will be discussed in more detail later.

## 1.2 Cyclodextrins

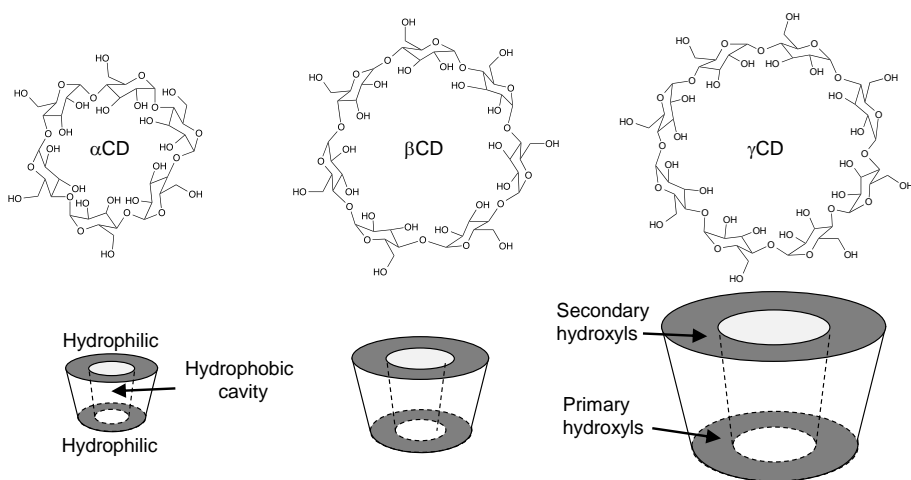


**Figure 2:** Molecular structure of  $\alpha$ -,  $\beta$ - and  $\gamma$ -cyclodextrin.

Cyclodextrins or cycloamyloses (CDs) are a group of sugar molecules bound together in a ring, see Figure 2. The sugar units are  $(\alpha-1,4)$ -linked  $\alpha$ -D-glucopyranose.[11] They are produced in nature during the bacterial digestion of starch. Based on the number of glucose residues in its structure, the different CDs are labelled with a Greek prefix. The three most common CDs are  $\alpha$ -,  $\beta$ - and  $\gamma$ -CD. They consist of six, seven and eight glucopyranose units, respectively. The glucopyranose units have taken a chair conformation, and as a result, the cyclodextrins take a truncated cone shape with an open centre. The hydroxyl groups are oriented towards the cones exterior. The primary hydroxyl groups are at the narrow edge of the cone and the secondary hydroxyl groups are at the wide edge. The carbon backbone and the ethereal oxygens are lining the cavity of the cyclodextrin that gives it a somewhat lipophilic nature and the outer area is hydrophilic.[12] The hydrophobic inside and hydrophilic outside of the CDs makes them ideal for inclusion (“host-guest”) complexes with hydrophobic molecules and enhance the solubility and bioavailability of these molecules. They have therefore been of interest for several industrial applications.[13–15] It is well known that CDs have interesting interactions with water, and the self-aggregation of CDs in solution is not fully understood.[16, 17] The solubility of  $\alpha$ -,  $\beta$ -, and  $\gamma$ -CD in water is low compared to other oligosaccharides, with values of 0.15, 0.016 and 0.18 M, respectively.[18] The dissolution of  $\beta$ -CD in water is disfavoured in terms of both entropy and enthalpy compared to  $\alpha$ - and  $\gamma$ -CD.[19] The solubility  $\alpha$ -,  $\beta$ - and  $\gamma$ -CD in  $D_2O$  is lower than in  $H_2O$ .[20] The anomalous solubility characteristics is suggested to be due to self-aggregation[21], effects on local water structure[22], differences in intramolecular ri-

gidity [23, 24], and water clustering inside the CD cavity.[25]

In the solid state, the interaction between CD and water is of great importance in the complicated relationship between different polymorphs and crystalline hydrates of CDs. Two structural motifs are known for CDs and their host-guest complexes.[12] They crystallize in either (a) a channel structure, in which the CD molecules stack in such a way that infinite channels are formed in the lattice; or (b) a cage structure, in which the CD molecules pack so that the cavity of each molecule is blocked by its neighbours, see Figure 3. The cage structures can be further subdivided into (b1) “brick” and (b2) “herringbone” types, depending on the exact packing of each molecule in the unit cell.

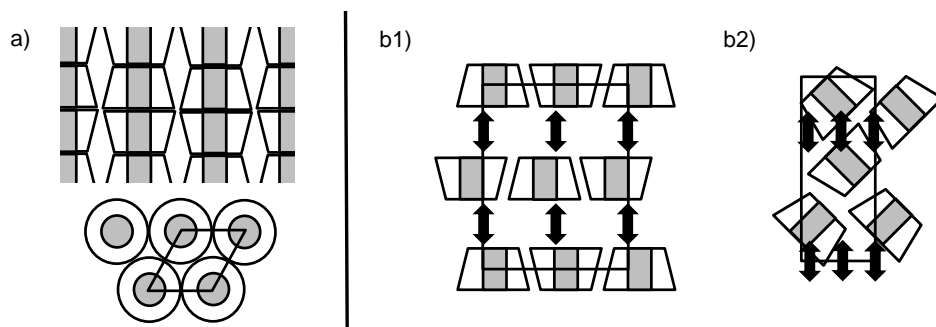


**Figure 3:** Schematic pictures of crystal packing motifs of cyclodextrin inclusion complexes: (a) channel, and cage-types (b1) brick, and (b2) herringbone from reference [12].

The crystal structures that are reported on CD systems are mainly host-guest complexes. In this study we focus on systems containing only  $\alpha$ -,  $\beta$ -, or  $\gamma$ -CD and water.  $\alpha$ -,  $\beta$ -, or  $\gamma$ -CD prefer to crystallise in a cage structure. However, a channel-type structure has also been observed under rapid crystallisation for  $\alpha$ - and  $\gamma$ -CD.[26–28]

No anhydrous crystalline phases have been reported for these CDs and the structures that have been reported vary in water content. It is also not uncommon that the structures are non-stoichiometric. CDs have an inherent capacity to host guest molecules and absorb water into their structures and still be stable, often without changing the unit cell dimensions.[29, 30] Single crystal data on several of these structures have been reported;  $\alpha$ -CD $\cdot$ 6H<sub>2</sub>O[31],  $\alpha$ -CD $\cdot$ 11H<sub>2</sub>O[32],  $\beta$ -CD $\cdot$ 11H<sub>2</sub>O[23],  $\beta$ -CD $\cdot$ 12H<sub>2</sub>O[33],  $\beta$ -CD $\cdot$ 10.5-12.0H<sub>2</sub>O[29],  $\beta$ -CD $\cdot$ 9.4-12.3H<sub>2</sub>O[30],  $\gamma$ -CD $\cdot$ 14.1H<sub>2</sub>O[34] and  $\gamma$ -CD $\cdot$ 17H<sub>2</sub>O[35]. It is not uncommon for CD structures to be reported more than once, and with different nominal composition, for instance  $\gamma$ -CD $\cdot$ 14.1H<sub>2</sub>O [34] and  $\gamma$ -CD $\cdot$ 13.3H<sub>2</sub>O.[36]

In a CD hydrate structure there are two types of water populations. Water molecules can reside inside the CD molecules cavity or outside in the interstices in the lattice.

This could be one reason for the varying amounts of water reported in the CD hydrate structures. For instance, Betzel et al[23] reported on the  $\beta$ -CD $\cdot$ 11H<sub>2</sub>O in a neutron diffraction study. They found that the hydrate structure contained 8 water inner cavity sites and 8 interstices on the outside. However, all possible water positions were not fully occupied. 6.13 water molecules are distributed in the inner cavity and 4.88 in interstices, yielding 11 water molecules (an undecahydrate). They also reported that the water molecules residing within the cavity are more ordered, “probably due to the hydrophobic character of the cavity”. In their study of the crystalline hydrate structure of  $\gamma$ -CD, Harata et al[34] reported that the structure is comprised of 14 water sites in the inner cavity and 9 interstitial sites on the CD molecule. In this structure, only 7.1 water molecules were found to occupy the inner cavity sites and 7.0 the interstitial sites.

Several water-induced polymorphic transitions in the CD hydrate structures have been observed. Nakai et al[37] reported on the solid-state behaviour of all the CDs over a wide range of water activity in their X-ray and sorption study. They found several solid-state phase transitions. Water-induced transitions have also been reported between channel and cage structures of  $\alpha$ -CD[27] and  $\gamma$ -CD[28], and between structures of a channel-type with tetragonal and hexagonal packing[38].

The rich polymorphism and the varying non-stoichiometric nature of the CDs suggest that their solid structures is a consequence of dynamic features. Betzel et al[23] reported on the “flip-flop” dynamics of the H-bonds in  $\beta$ -CD, whereas Steiner et al[30] and Kitchin et al[39] investigated the water diffusion between different sites and different populations in  $\beta$ -CD. They all find rapid dynamics and high water mobility in the crystalline  $\beta$ -CD structure. Hunt et al theorize that a high degree of dynamics characterise the CD part of the structures.[28]. However, there is not enough experimental data that supports this claim.

### 1.3 Cellulose

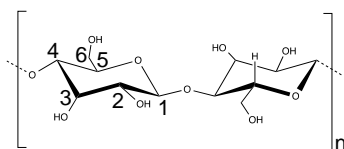


**Figure 4:** Molecular structure of the repeat unit of cellulose with  $^{13}\text{C}$  labelling.

Cellulose is the most abundant natural polymer on our planet as it is the main component of plant cell walls. It is a polysaccharide usually consisting of a couple of hundred to several thousand linked sugar units, or more specifically  $\beta$ (1-4) linked *D*-glucose residues, see Figure 4. Natural cellulose is denoted cellulose I, and consists of structures  $I_\alpha$  and  $I_\beta$ . [40, 41] Cellulose can form other crystalline structures by chemical treatments. By dissolution or coagulation (regenerated), or swelling (mercerization) cellulose I will irreversible form the crystalline allomorph cellulose II. [42] A difference in structure between Cellulose I and II, is that cellulose I has all-parallel (aligned) chains and cellulose II has anti-parallel (alternating) chains. [43, 44]

Cellulose is hydrophilic but is well known for its insolubility in water and most organic solvents. However, it can be dissolved in solvents with intermediate features, like *N*-methylmorpholine *N*-oxide and ionic liquids. Cellulose can be dissolved in water but only at high and low pHs, and preferably together with an additive. [45] In literature [46], one view is that this insolubility in water is due to extensive intermolecular hydrogen bonding between adjacent polymer chains in the solid state. Recently, Lindman et al [45] published an analysis of the intermolecular interactions and mechanisms governing cellulose dissolution, that challenges this view. In the so-called "Lindman hypothesis" they emphasize the importance of the amphiphilic nature of cellulose. The hydrophobic interactions between the hydrophobic patches in the cellulose is argued to be important with regards to cellulose aqueous insolubility.

Cellulose is one of the most important commercial raw materials in the world due to its wide range of applications, so from an economical and environmental perspective, dissolution media based on water are strongly preferred. Traditionally, cellulose dissolution has been a non-environmentally friendly process. One area that has advanced in recent years is the use of ionic liquids that have proven to be very effective in dissolving cellulose. [47] They have high thermal and chemical stability, and are miscible with several other solvents. However, many systems have shown great limitations when it comes to industrial uses which is a huge drawback. Many cellulose systems form gels

upon water addition. These gels might hold the answer to the fundamental mechanisms behind cellulose dissolution in aqueous solutions.

## 1.4 Polymer electrolyte membranes

It is well known that there is a big demand for new energy sources. The fossil fuels have for a long time been the primary energy source in the world. However, fossil fuels are a non-renewable resource and the reserves are going to run out. Also the fossil fuels have been shown to be a big contributor to the greenhouse effect, and therefore linked to increased global warming. An alternative power source are fuel cells. Fuel cells have been of great interest since their discovery in the late 1830's. A fuel cell is an electrochemical device that can continuously convert chemical energy of a fuel into electrical energy in a clean and efficient way. There are different types of fuel cells but they all consist of an anode and a cathode, as well as an electrolyte that enables charge transport. The charge carrier varies in the different types of fuel cells but hydrogen (proton) is common.

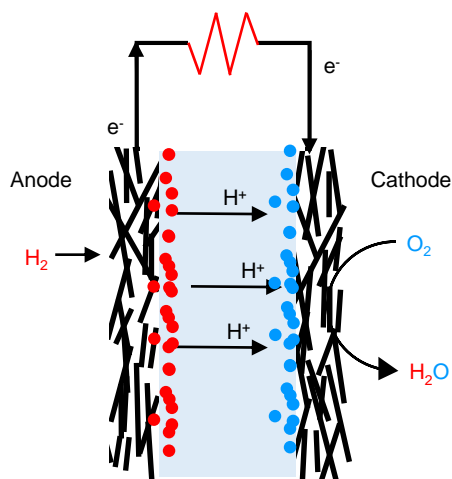


**Figure 5:** Schematic drawing of a polymer electrolyte membrane fuel cell (PEMFC). A solid polymer membrane in the centre serves as separator and electrolyte. Fibrous carbon electrodes allow the transport of electrons, reactants, and water to and from the reaction zone, which contains highly dispersed platinum particles supported on high-surface-area carbon as the electrocatalyst.

Ion-containing polymers can be used as electrolyte membranes for electrochemical fuel cells. These kinds of polymer electrolyte membrane fuel cell (PEMFC) can be used in applications such as portable electronics, remote power sources, and electric vehicles. In Figure 5 is a schematic picture of a PEMFC. The electrochemical reaction of hydrogen and oxygen occurs in two half-cell reactions separated by a solid polymer electrolyte or proton-exchange membrane (PEM). The hydrogen atoms are oxidised at the anode and pass to the cathode via the PEM. At the cathode an oxygen reduction occurs. The PEM is the most important part of the fuel cell and it has several requirements that need to

be fulfilled. It needs to be impermeable to the reactant gases (such as oxygen or hydrogen), mechanically and chemically stable, have high proton conductivity, low (or no) electron conductivity, have balanced water transport and they need to have reasonable production costs. In order to produce ion-containing polymers for electrolyte applications it is important to improve our understanding of the complex structure-property relations.[48]

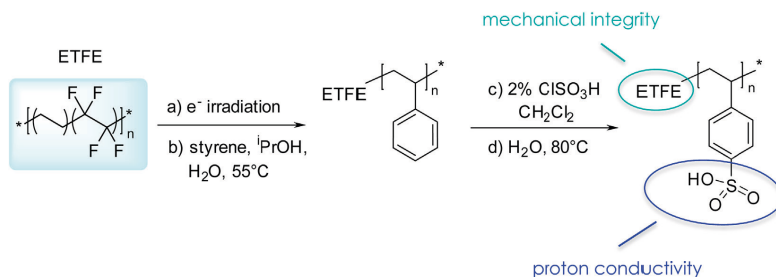


**Figure 6:** The chemical structure of ETFE-g-poly(styrenesulfonic acid-co-methacrylonitrile) polymer electrolyte. The scheme shows the synthetic pathway for proton conducting membranes with a backbone structure of a ETFE base film with mechanical integrity and strength and functional groups for proton conductivity.

These membranes can be created through radiation grafting, which gives high design flexibility, enabling a fast and efficient product development of electrochemical applications. Figure 6 illustrates a schematic picture of an ETFE-g-poly(styrenesulfonic acid-co-methacrylonitrile) (ETFE) polymer electrolyte base film. By irradiating a ETFE base film using electron beam technology (a) it is possible to produce reactive sites in the starting material. These sites are then allowed to react with selected monomers (b-d) which produce well-defined membranes with a backbone structure of ETFE base film. This gives mechanical integrity and strength and adds functional groups for proton conductivity.[49, 50] The microstructure of the extruded ETFE base film is inherently anisotropic due to the manufacturing process.[51] For instance, if the extrusion occurred in the machining direction (MD) or in the transverse direction (TD) is expected to greatly affect the final performance of the PEM.[48] Grafted membranes seem to hold much promise for PEFC applications.[52–56] However, knowledge of the impact the structure and the morphology of the polymer has on functions, such as proton mobility and conductivity, is still rather limited.[48, 57]

## 2 Experimental methodology

To characterize solid samples one often needs to use several different techniques such as NMR techniques, X-ray scattering techniques and gravimetric techniques. A brief description of the experimental techniques used in this thesis work will follow.

### 2.1 Sample preparation

Saturated salt solutions can be used to hydrate materials through the vapor-phase to specific relative humidity (RH) at fixed temperature[58], see Figure 7.

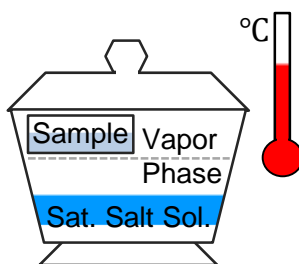


**Figure 7:** Desiccator with saturated salt solution yielding a specific hydration level of the vapour phase at a specific temperature.

### 2.2 Nuclear Magnetic Resonance (NMR)

Nuclear Magnetic Resonance (NMR) spectroscopy[59] is a technique that is based on the interaction of electromagnetic radiation with atomic nuclei. It is a technique routinely used in science when studying physical, chemical and biological properties of matter. It further enables us to study molecular structure and motion as well as chemical reactions. NMR uses the fact that atomic nuclei possess a property called spin. Only nuclei with non-zero spin are NMR active. Neutrons, protons, electrons and  $^{13}\text{C}$  all possess a nonzero spin  $1/2$ . Atomic nuclei with non-zero spins will behave as a small magnet if they are subjected to a magnetic field. The most common atomic nuclei investigated with NMR are  $^1\text{H}$  (protons) and  $^{13}\text{C}$ . The natural abundance of protons is high (around 99 %) while  $^{13}\text{C}$  has a very low natural abundance (around 1 %). When placed in an external magnetic field,  $B_0$ , the spins will align more parallel to  $B_0$ , creating a bulk magnetization ( $M$ ) along the longitudinal  $z$ -axis. The  $x$ - and  $y$ -axes are perpendicular to the  $z$ -axis and together they form the transverse plane.  $M$  can conveniently be seen as a vector, or spin packet of magnetization, precessing around the

$z$ -axis at the Larmor frequency,  $\omega_0$ . Applying a radio frequency (rf) pulse relative to the  $z$ -plane on the  $M$  causes it to flip away from the  $z$ -axis onto the transverse plane. When a combination of pulses is used it is called a pulse sequence. After the rf pulse  $M$  returns to equilibrium. A NMR signal deteriorates with two separate processes. The longitudinal relaxation time constant,  $T_1$ , is responsible for the loss of signal intensity. The transverse relaxation time constant,  $T_2$ , is responsible for the broadening of the signal and loss of intensity by dephasing the spins. The time constants  $T_1$  and  $T_2$  are connected to how fast a molecule reorients or tumbles. This is referred to as the correlation time. Since smaller molecules can reorient faster they have shorter correlation times.

The free induction (FID) decay signal is recorded as a function of time. By Fourier transformation the signal is converted to the frequency domain. The resonance frequencies of all nuclei are not identical due to the fact that they depend on the local electron distribution which is different at different positions in the molecule. This is called chemical shift,  $\delta$ , and it is what makes NMR so useful in molecular structure analysis because it allows us to distinguish between different types of atoms present in the molecule. Usually the chemical shift is referenced with respect to a standard chemical shift. Reporting the chemical shift in this way has the advantage that data measured at different magnetic fields can be compared. Usually, spectra are plotted with the ppm scale increasing from the right to the left. The chemical shift range for protons are typically 0-10 ppm and for carbons it is 0-250 ppm.

In a molecule the different spins do not precess independently. There are two types of couplings between spins; scalar and dipolar couplings. Scalar couplings or J-couplings are mediated through the bonds. If the nuclei are up to three bonds away from each other they may affect each other's effective magnetic field. Dipolar coupling are mediated through space with strength  $1/r^3$  with a distance,  $r$ , between the interacting nuclei. Both the scalar and dipolar couplings can occur between the same kind of nuclei (homonuclear coupling) or between two different kinds of nuclei (heteronuclear coupling). Natural  $^{13}\text{C}$  systems are magnetically dilute so homonuclear couplings pose little problem (still a problem in  $^1\text{H}$  spectra). Heteronuclear decoupling schemes are available to use during signal acquisition. Typically C-H couplings are in the range of 125 Hz and C-C couplings are in the range of 33 Hz.

A very useful application in NMR experiments is the Magic Angle Spinning (MAS). The sample is spinning at the magic angle,  $\theta$ , of approximately  $54.74^\circ$  with respect to the direction of the external magnetic field. By using MAS one can modify the spectra to get better resolution. The MAS suppresses chemical shift anisotropy, homonuclear and heteronuclear dipolar couplings.

## Polarization Transfer solid state NMR (PTssNMR)

The Polarization Transfer solid-state NMR technique (PTssNMR) is a high-resolution solid-state NMR method that can be used to enhance the signals intensities in cases where the nuclei of interest have low inherent sensitivity due to low natural abundance or gyromagnetic ratio. A signal enhancement can be achieved by transferring the polarization from an abundant spin (in our case  $^1\text{H}$ ) to the rare spin (in our case  $^{13}\text{C}$ ) which is of interest. In their newly developed PTssNMR methodology, Nowacka et al [10, 60] have shown that successive measurements of the  $^{13}\text{C}$  direct polarization technique (DP), the cross polarization technique (CP) and the insensitive nuclei enhanced by polarization transfer (INEPT) is a powerful scheme to study complex materials containing solid, liquid, and liquid crystalline domains.

They have developed a theoretical model[10, 60] for their method that predicts the signal intensities, see Figure 8d. The CP and the INEPT signal intensities is expressed as a function of the generalized CH-bond orientational order parameter ( $S_{CH}$ ) which is a measure of anisotropy in the system and the CH-bond re-orientational correlation time ( $\tau_{CH}$ ) which describes the motion or the reorientation of the molecule.

The  $^{13}\text{C}$  DP NMR technique gives information about all the  $^{13}\text{C}$  atoms present in the system. It is, with sufficiently long recycle delays compared to the  $T_1$ , quantitative and proportional to the number of  $^{13}\text{C}$  nuclei giving rise to a peak. It may be viewed as a reference to CP and INEPT. The peak widths depend on the  $T_2$ , the magnetic field homogeneity, the MAS rate and  $^1\text{H}$  decoupling. The  $^{13}\text{C}$  signal is acquired during high-power  $^1\text{H}$  decoupling and MAS. In the CP measurements the polarization transfer occurs through dipolar coupling, an interaction through space.

In INEPT the polarization transfer occurs through the scalar couplings, an interactions through the bonds. The signal acquired will be a result of the dynamic state a specific segment is in. While CP is a typical method used of signal enhancement of more rigid segments, INEPT is used for signal enhancement of more liquid-like segments.

The signals acquired in CP and INEPT are compared to DP and chemical shifts gives information about molecular structure, conformation, and packing and the signal intensities from the CP[61] and INEPT[62] gives information about molecular dynamics.

The model in Figure 8d by Nowacka et al [10, 60] predicts that solids, with  $\tau_c > 0.1$  ms, give CP  $\gg$  INEPT = 0. Isotropic liquids, with  $\tau_c < 1$  ns and  $S_{CH} < 0.01$ , yield INEPT  $\gg$  CP = 0. For anisotropic liquids, there is a gradual increase in the CP-to-INEPT ratio when increasing  $S_{CH}$  in the range from 0.01 to 0.5. At  $S_{CH} \approx 0.1$ , the two techniques give equal signal intensities. In the intermediate dynamical regime,

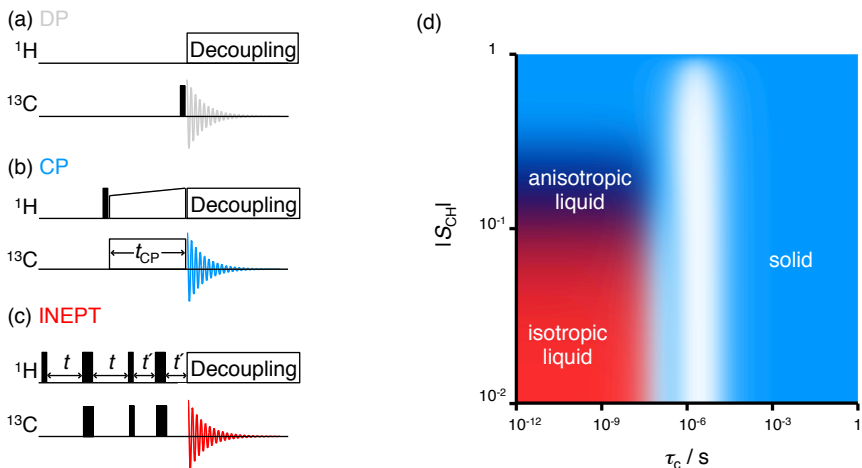


**Figure 8:** Polarization transfer solid state NMR (PTssNMR) pulse sequences (a–c). DP (grey) from direct polarization of  ${}^{13}\text{C}$ , while CP (blue) and INEPT (red) involve polarization transfer from  ${}^1\text{H}$  to  ${}^{13}\text{C}$ , all with acquisition of  ${}^{13}\text{C}$  signal during  ${}^1\text{H}$  decoupling and magic-angle spinning (MAS). Narrow and broad vertical lines indicate  $90^\circ$  and  $180^\circ$  radio-frequency pulses, respectively. Figure (d) Theoretical signal intensity enhancement vs. the CH-bond orientational order parameter  $S_{CH}$  and reorientational correlation time  $\tau_c$  for CP and INEPT. Isotropic liquids are visualized with only INEPT, anisotropic liquids with both INEPT and CP, and solids with only CP. The white area indicates where neither CP and INEPT is present.

$\tau_c \approx 1 \mu\text{s}$ , neither CP nor INEPT are present.

Since its development the method has been successful in investigating amphiphilic systems which are difficult to characterize due to their wide range of solid and liquid crystalline phases, and co-existence phases between them. The PTssNMR technique has been used on hydrated surfactants,[10, 60] lipid biomembranes,[63] lipid-amyloid fibril aggregates,[64] and intact stratum corneum,[65–67] and cellulose dissolution[68, 69].

## Pulsed Field gradient NMR

Pulsed field gradient (PFG) NMR is an experimental technique which is used to investigate the mobility/transport of liquid or liquid-like substances. PFG NMR uses the strength of the magnetic field to mark the spins with a position by applying a magnetic field gradient and measure the displacement after the spins have undergone Brownian motion. There are two main pulse sequences PFG spin echo (PFGSE) and PFG stimulated spin echo (PFGSTE). The former is limited by  $T_2$  relaxation and the latter mainly by  $T_1$  relaxation. For water-poor systems with solid-like properties, where  $T_2 \ll T_1$ , PFGSTE is the method of choice. Figure 9 illustrates the PFGSTE pulse sequence. The self diffusion coefficient  $D_{\text{self}}$  can be estimated from the NMR-signal, echo attenuation  $E$ , by fitting the experimental data to the Stejskal-Tanner equation[70]

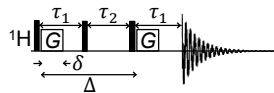


**Figure 9:** The NMR diffusometry pulsed field gradient stimulated echo experiment. The three narrow vertical lines indicate the  $90^\circ$  radiofrequency pulses. The gradients with amplitude  $G$  during time  $\delta$  are located after the first and third  $90^\circ$  radiofrequency pulses. The diffusion time  $\Delta$  between starting edges of the gradient blocks, with an effective diffusion time of  $\Delta - \delta/3$ .

$$E(b) = E_0 \exp(-bD_{\text{self}}) \quad (1)$$

where  $b = \gamma^2 \delta^2 G^2 (\Delta - \delta/3)$ . An important fact to keep in mind when performing NMR diffusion measurements on hydrated carbohydrate systems is that there can be cross-relaxation effects occurring between the solid and the liquid pools. If that is the case, Equation (1) has to be modified with a cross-relaxation term.[71]

### 2.3 Powder X-ray diffraction (PXRD)

A common technique to use for structure determination is Powder X-ray diffraction (PXRD). It allows us to investigate the sample on the Ångström lengthscale (nm). When X-rays are scattered by the electron clouds of the atoms in the sample, a characteristic diffraction pattern is produced as a function of the scattering angle ( $2\theta$ ). Every observed reflection in the diffraction pattern satisfies Bragg's law

$$n\lambda = 2d \sin(\theta) \quad (2)$$

where  $n$  is the order of diffraction,  $\lambda$  is the wavelength of the X-ray source, and  $d$  is the interplanar distance.

Crystallographic information files (cif) from the Cambridge Structural Data (CSD) base was transformed into theoretical diffraction patterns.[72–74] The experimental data was compared to the theoretical pattern to identify the crystalline phases in the samples.

## 2.4 Dynamic Sorption Balance

Dynamic Sorption Balance is a gravimetric technique that is used to measure vapour sorption isotherms. The determination of the amount and speed of adsorption is very important in many industrial areas like pharmaceuticals, foods, hygiene products, construction material, fuel cells.

Most common are water sorption isotherms. The sample's mass change is measured on a microbalance at constant temperature during a step-wise increasing/ or decreasing ramp of hydration level. The amount of water is often expressed as relative humidity (RH) which is related to the water activity  $a_w$  through

$$RT \ln \left( \frac{RH}{100} \right) = RT \ln (a_w) = \Delta\mu_w = -\frac{1}{V_w} \Pi_{\text{osm}} \quad (3)$$

where  $\Pi_{\text{osm}}$  is the osmotic pressure,  $T$  is the temperature and  $V_w$  is the volume of water.

## 2.5 Thermogravimetric Analysis

Thermogravimetric analysis (TGA) is a technique frequently used in science for characterization of materials and determining physical and chemical properties. By following the weight-change of a material as a function of controlled heating, or isothermally over time, in a controlled atmosphere one can follow phase transitions due to dehydration, oxidation or decomposition.[75]

### 3 Main results of the research papers

#### Paper I Equilibrium and non-equilibrium phases of alkylglycoside *n*-tetradecyl- $\beta$ -D-maltoside in the water-poor regime

In this study the phase behaviour of the  $C_{14}G_2/H_2O$  system is investigated. Focusing on the structure and molecular dynamics of the different solid phases. A series of solid phases were prepared according to the protocols of Ericsson et al[8]. The structures were verified with X-ray diffraction data by comparison with previously published results from [8]. The solid structures were exposed to moisture through equilibration in contact with saturated salt solutions with varying RH at 25°C and the water content was determined gravimetrically. The  $^{13}C$  PTsNMR method[10, 60] was used to follow the structures with respect to hydration level and temperature.

Ericsson et al[8] have proposed structures of the solid  $C_{14}G_2/H_2O$  phases, see Figure 10. All the solid phases have a lamellar structure with alternating alkyl-chain and maltoside layers. However, they differ in water content and in the packing of the hydrophilic and hydrophobic parts of the molecule. The liquid crystalline ( $L_\alpha$ ) and glass ( $L_g$ ) phases have disordered alkyl-chains while the other structures have interdigitated alkyl-chains with all-trans conformation. The alkyl-chains are tilted with respect to the layer normal for the ordered lamellar phase ( $L_\beta$ ), the anhydrous low-temperature crystalline phase (AH1), and the hemihydrate crystalline phase (HH). A new phase was found and verified gravimetrically to be a dihydrate (DH). A phase diagram was constructed on the basis of structure of starting material, RH, and temperature.

As discussed in the experimental section, the experimental observables in PTsNMR are the chemical shifts, linewidths, and amplitudes of the  $^{13}C$  resonance lines. The values of the chemical shifts and peak amplitudes give information on molecular conformation and dynamics, both factors being determined by the molecular organization and packing in the phases. The DP spectra is indicated with grey, CP with blue, and INEPT with red traces. CP or INEPT signal intensities indicate solids or isotropic liquids, respectively. The presence of both CP and INEPT signal intensities, with comparable amplitudes, indicates an anisotropic liquid state of the molecular segment, and is visualised in purple colour. Figure 10 summarises all the observed structures of  $C_{14}G_2/H_2O$  in the water-poor region. The carbon labelling is given in the molecular structure of  $C_{14}G_2$  drawn on top of Figure 10.

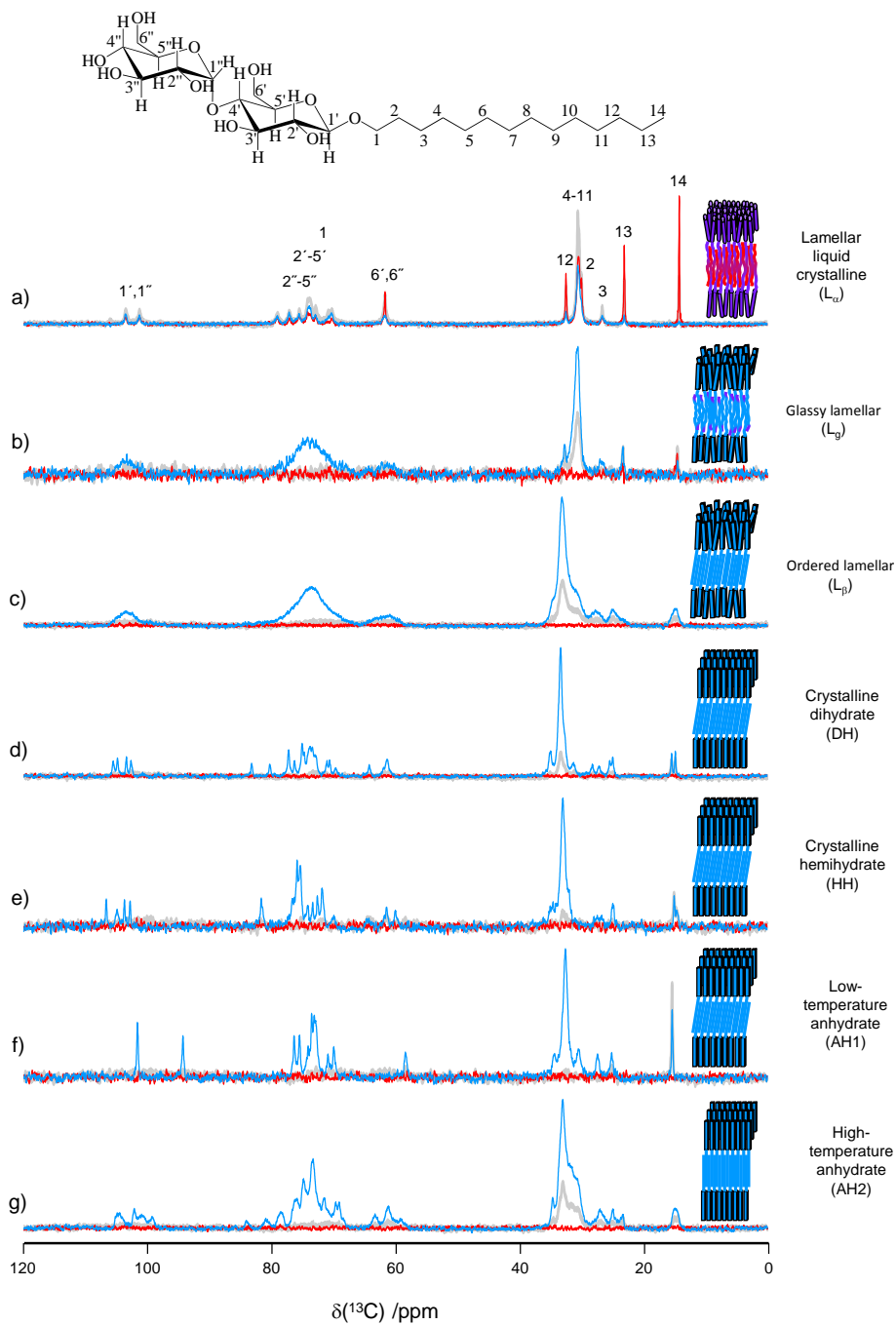


**Figure 10:**  $^{13}\text{C}$  PTsNMR spectra of all the  $\text{C}_{14}\text{G}_2/\text{H}_2\text{O}$ -phase observed in the water-poor regime. Spectra were acquired at  $B_0=11.74$  T with 5 kHz magic-angle spinning and 68 kHz TPPM  $^1\text{H}$  decoupling. DP (grey), CP (blue), and INEPT (red) spectra are shown together with redrawn phase structures from the paper by Ericsson et al.[8]. The structures are color-coded with the observed CP(blue) and INEPT(red) signal intensities and the purple colour represents the presence/ratio of CP and INEPT intensities when both are present. The  $^{13}\text{C}$  peak assignment in spectrum (a) refers to the carbon  $^{13}\text{C}$  labelling in the molecular structure of  $\text{C}_{14}\text{G}_2$  drawn on top.

In Figure 10a is a spectra of the anisotropic liquid crystalline  $L_\alpha$  phase. The  $^{13}\text{C}$  resonance lines were assigned with the help of literature from Sjögren et al on the *n*-dodecyl-D-maltoside ( $\text{C}_{12}\text{G}_2$ ) in acetate buffer[76] and Nowacka et al on the *n*-octyl-D-maltoside ( $\text{C}_8\text{G}_2$ )  $L_\alpha$  phase.[10] The  $^{13}\text{C}$  chemical shifts from the alkyl chain appears in the range 10-40 ppm, and  $^{13}\text{C}$  chemical shifts from the head-group appear in the range 55-110 ppm. Both CP and INEPT signals are present in most of the peaks in approximately equal amounts, with a  $S_{\text{CH}}$  around 0.1. In  $\text{C}_{12}$ ,  $\text{C}_{13}$ , and  $\text{C}_{14}$  the INEPT dominates. These carbons segments are located at the end of the alkyl chain and they reorient nearly isotropically. The long alkyl chain,  $\text{C}_{4-11}$ , has a peak at 30.5 ppm, has liquid-like distribution of both *trans*- and *gauche* conformers.[77]



The  $L_g$  phase is not so different from the  $L_\alpha$  phase when it comes to the structure. It differs in the dynamics.[9, 10] The  $L_g$  is dominantly represented by CP and therefore in a solid state, see Figure 10b. However, some INEPT signals are present. At the end of the alkyl chain,  $\text{C}_{14}$  and  $\text{C}_{13}$ , the segments reorient with  $\tau_c$  as low as nanoseconds. Walderhaug et al [78] showed that the  $\tau_c$  and  $S_{\text{CH}}$  in alkyl chains, in surfactant aggregates, gradually decreases with an increase in the distance of the segment to the head-group. This smooth decrease in  $\tau_c$  can be several orders of magnitude.[10] An increase in temperature of an  $L_g$  phase leads to a gradually lower  $\tau_c$  and a continuous transition into a  $L_\alpha$  phase.[10] The non resolved head-group peaks indicates that there is no organized molecular packing of those segments in the  $L_g$  phase. As for the  $L_\alpha$  phase, the long alkyl chain ( $\text{C}_{4-11}$ ) has a peak at 30.5 ppm in accordance with a *trans*- and *gauche* conformation.



No INEPT signal is present in the spectra in Figure 10c-g. These phases are solid with molecular segments with  $\tau_c > 0.1$  ms. In contrast to the  $L_\alpha$  and  $L_g$  phases, the long alkyl chain ( $C_{4-11}$ ) peak has shifted from 30.5 ppm to 33.5 ppm. This is consistent with the alkyl chains being in an all-trans conformations.[79] The phases in Figure 10c-g all have well-ordered packing of molecules with finite number of possible conformations yielding sharp CP resonance lines. All phases except the ordered lamellar phase have resolved head-group peaks, see Figure 10c. This indicates a well ordered molecular arrangement in the head-group.

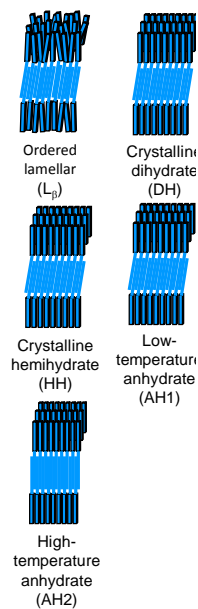
The spectra for DH and HH phases, see Figure 10d and 10e show signs of two non-equivalent sites being present in the crystal unit cell in the doubling of the resonance lines. The anhydrous high-temperature (AH2) sample show signs of contamination with an amorphous phase. If more than one phase is present there will be a superposition of the two phases.

PTssNMR gives characteristic spectra for the different phases, much like a fingerprint. However, it is no possible to deduce more precise information about the crystal structure through PTssNMR but it is a good complement to PXRD. The quality and purity can also be determined from the  $^{13}\text{C}$  resonance lines.

The stability investigation was performed on the anhydrous  $L_g$ ,  $L_\beta$ , AH1, and AH2 phases after equilibrating them for two weeks over supersaturated salt solutions at 25 °C generating different RH. Gravimetric determination of water content was performed and  $^{13}\text{C}$  PTssNMR was used for characterisation by using reference spectra from the starting materials determined previously with PXRD (Figure 10). The temperature was ramped from 2-58 °C after an initial measurement at 25 °C.

The AH1 phase remains stable in our investigated RH and temperature range. Hydrating the  $L_g$  at surfactant concentrations below 96 wt% results in the formation of the DH phase. As expected,  $L_g$  in the dry state gradually transforms into the  $L_\alpha$  phase. This is in agreement with the calorimetric glass transition temperature (48 °C) determined by Ericsson et al[8].

The glass transition appears higher in NMR than in DSC measurement, and above the temperature range investigated here.[10] The only difference between the  $L_\alpha$  and  $L_g$  phases that we can detect is in the dynamics (not structure). Therefore,  $L_\alpha$  and  $L_g$  are regarded as one in the following discussion. Upon heating the DH phase melts into  $L_\alpha/L_g$ .



Hydrating the  $L_\beta$  phase at 25 °C leads to a formation of the DH at a surfactant concentration of 94 wt%.  $L_\beta$  in the dry state melts into  $L_\alpha/L_g$  at 39 °C compared with at 54 °C reported by Ericsson et al[8] in their DSC study. The sample can have absorbed some more moisture during sample preparation for NMR measurements resulting in a lower transition temperature. As expected, cooling the  $L_\alpha/L_g$  phase gradually slows down the dynamics and the  $L_g$  becomes more prominent and there is no reformation of the  $L_\beta$  phase.

At a surfactant concentration of 95 wt% the  $L_\beta$  phase transitions into a two-phase region with  $L_\alpha/L_g$  and DH at temperatures above 39 °C. When cooling again the two-phase system remains stable. The DH phase with 95 wt% surfactant concentration is unaffected temperature. However, the DH phase with 90 wt% surfactant concentration partially melts into  $L_\alpha/L_g$  at 58 °C. Heating the AH2 phase in the dry state to temperatures above 25 ° there is a phase co-existence between the AH2 and  $L_\alpha/L_g$ . Hydrating the AH2 phase at 94 wt% surfactant concentration leads to a formation of the DH phase. Upon heating a transition into the two-phase region with DH and  $L_\alpha/L_g$  occurs. AH1 in the dry state and the DH phase with 94 wt% surfactant concentration partially melt into  $L_\alpha/L_g$  at 25 and 39 °C, respectively. The two-phase DH+ $L_\alpha/L_g$  system with 86 wt% surfactant concentration forms a pure  $L_\alpha/L_g$  phase at 48 °C.

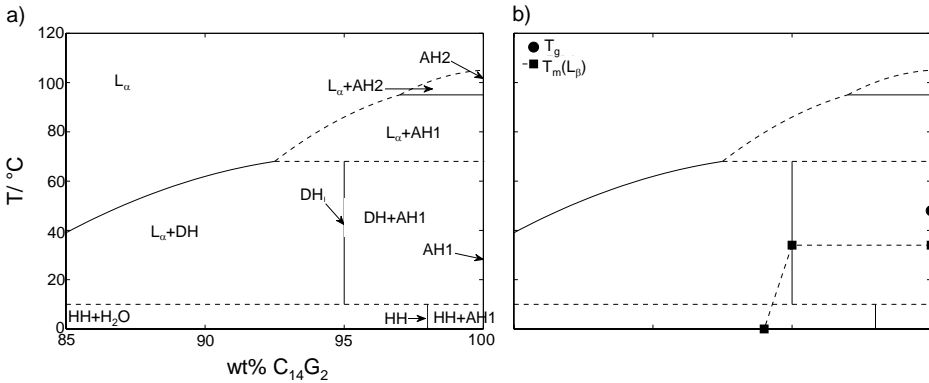


**Figure 11:** Phase diagram of the solid phases of  $C_{14}G_2/H_2O$  in the water-poor regime with respect to composition and temperature. (a) Visualizes an equilibrium phase diagram with the lamellar liquid crystalline phase ( $L_\alpha$ ), anhydrous low-temperature crystalline phase (AH1), anhydrous high-temperature crystalline phase (AH2), hemihydrate crystalline phase (HH), and the dihydrate crystalline phase (DH). Dashed lines are given for approximated phase boundaries. (b) Visualizes the regions of metastability of the non-equilibrium ordered lamellar phase ( $L_\beta$ ) and glassy phase ( $L_g$ ) within the equilibrium phase diagram. The  $L_\alpha/L_g$  calorimetric glass transition temperature  $T_g$  and the  $L_\beta$  melting points  $T_m$  are indicated by a circle and squares, respectively.

Combining the results from this study with previously reported data by Ericsson et al,[8] enables us to construct an equilibrium phase diagram (Figure 11a), together with the non-equilibrium phases that are at least metastable (Figure 11b). Starting with what we know from previously reported data by Ericsson et al TGA, PXRD and NMR ex-

periments have shown that the anhydrous AH1 phase precipitates at 22 °C from supersaturated solutions. The Krafft point, the minimum temperature for micellization, of the AH1 solution occurs at 32 °C. On the other hand, at 6 °C it is the HH phase that precipitates. From this we conclude that we have a one phase region of HH at 98 wt% and one at of AH1 at 100 wt%. Due to these facts we expect to have a phase boundary between HH and AH1 somewhere between 6 and 22 °C. Arbitrarily indicated with a dashed line at 10 °C. Above the Krafft point of AH1, there is a co-existence region of the DH phase together with either  $L_\alpha$  or AH1. The phase boundary between the pure  $L_\alpha$  phase and the co-existence area of  $L_\alpha$ +DH was found to exist between approximately 40 °C at 85 wt% and 70 °C at 92.5 wt%, indicated with a smooth solid line.

Ericsson et al[8] reported on the anhydrous AH2 phase. With SAXS, PXRD and DSC it was found to be stable between 95 and 105 °C, forming a one phase region of AH2 between these temperatures. A co-existence phase between AH2 and  $L_\alpha$  is outlined in the phase diagram from this study. NMR and gravimetric verifies the presence of the DH phase, and the NMR data implies that it occurs somewhere above 58 °C.

The phase diagram of  $C_{14}G_2/H_2O$  at low water contents was determined in this study.  $^{13}C$  PTssNMR is a powerful complement standard techniques such as PXRD, SAXS, and TGA when characterizing complex organic solid/ and semi-solid systems at low water contents.

## Paper II Effect of Water Activity on the Structure, Dynamics and Hydration of Crystalline $\alpha$ -, $\beta$ -, and $\gamma$ -Cyclodextrin

In paper II we investigated the influence of water activity on the stability of crystalline hydrates of  $\alpha$ -,  $\beta$ -, and  $\gamma$ -cyclodextrin (CD) by using gravimetric techniques and X-ray diffraction together with Polarization Transfer solid state Nuclear Magnetic Resonance (PTsNMR) techniques.

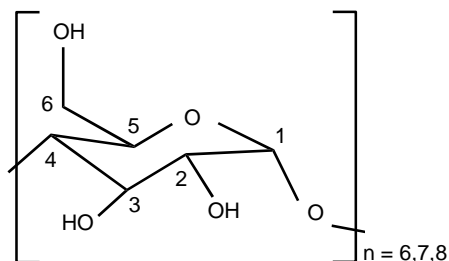


**Figure 12:** Molecular structure of the repeat unit of cyclodextrin with  $^{13}\text{C}$  labelling.  $\alpha$ -,  $\beta$ - and  $\gamma$ -CD consist of six, seven and eight glucopyranose units.

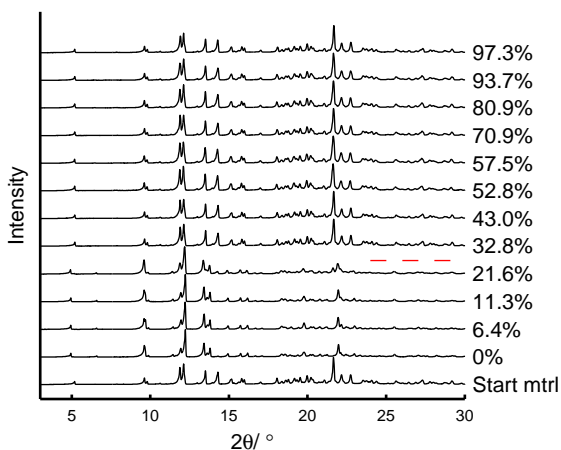


**Figure 13:** X-ray diffractograms at ambient temperature of  $\alpha$ -CD starting material and equilibrated at increasing water activity in units of relative humidity. The dashed red line indicates a solid-state phase transition.

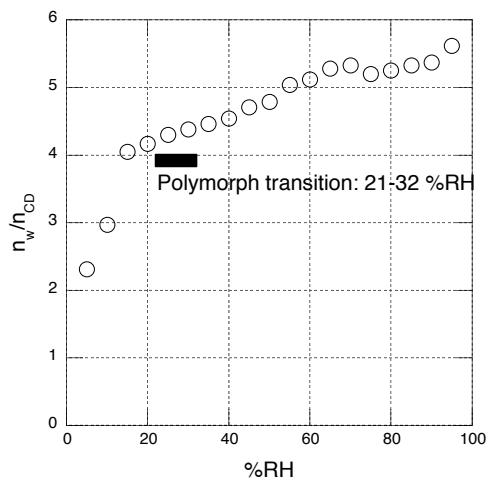


**Figure 14:** GVS data on  $\alpha$ -CD, given as the number of water molecules per CD molecule, as a function of relative humidity. The bar indicates the solid-state transition region indicated in the PXRD data in Figure 13.

### $\alpha$ -CD

In Figure 13 are X-ray diffractograms of  $\alpha$ -CD at different water activities ranging between 0 and 97.3 %RH and the starting material at ambient temperature. Between 21.6 and 32.8 %RH a change is observed in the diffraction patterns indicating a solid phase transition. Water sorption data close to this solid-solid transition range reveal a sharp jump in the water adsorption isotherm, see Figure 14. The discrepancy between the two techniques can probably be attributed to kinetic factors. In the PXRD measurements the samples are equilibrated for several weeks and in the GVS the isotherm was recorded over a shorter time scale of a couple of days and hence, the “overshoot” in the GVS data. Recrystallization is not an instantaneous process. At 4 water molecules per CD molecule there is an inflection point. One hypothesis is that this corresponds to the amount of water that can fit into the CD cavity and that additional water induces structural changes driven by the necessity to accommodate the additional water molecules into the interstices in the crystal lattice. Going up to higher water activity the adsorption isotherm eventually levels out at 6 water molecules per CD molecule.

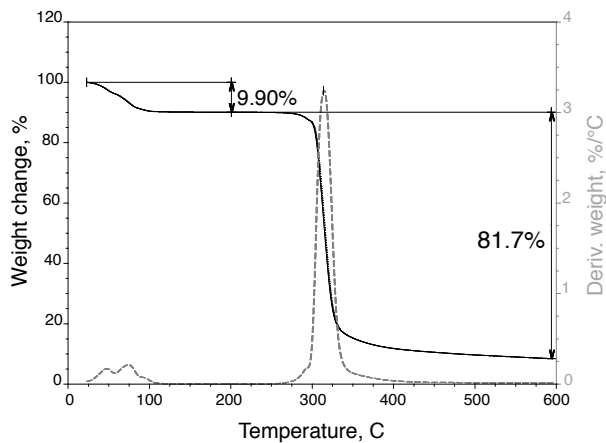


**Figure 15:** TGA data on  $\alpha$ -CD equilibrated at 11.3 %RH (LiCl). The initial mass loss of 9.90 % corresponds to 5.93 water molecules per CD molecule.

TGA data confirm this level of hydration on material equilibrated at 11.3 %RH (LiCl), see Figure 15. The amount of water also agrees with the  $\alpha$ CD-6H<sub>2</sub>O hydrate that has previously been characterised by Klar et al[31, 72–74].

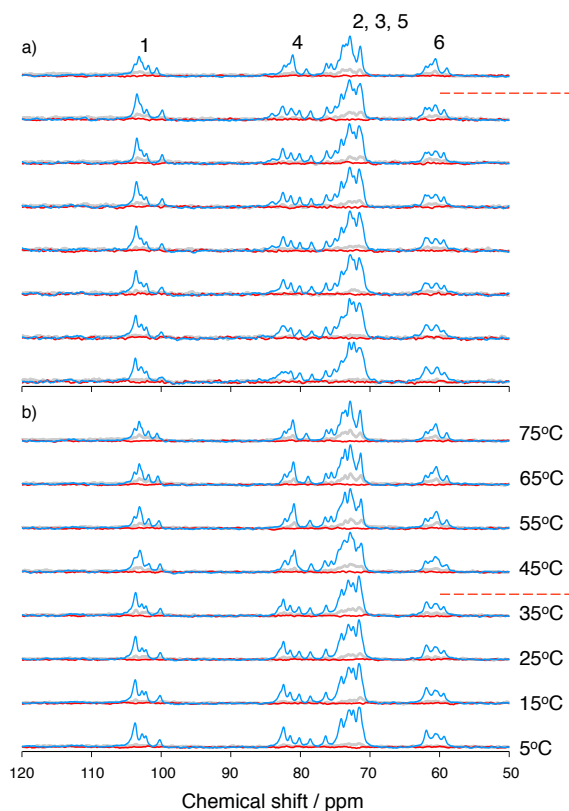


**Figure 16:** Solid-state  $^{13}\text{C}$  PTssNMR spectra of  $\alpha$ -CD at different temperatures equilibrated under dry conditions (a) and at 6 %RH (b). Spectra acquired at  $B_0=11.74$  T with 5 kHz magic-angle spinning and 68 kHz TPPM  $^1\text{H}$  decoupling. DP, CP, and INEPT spectra are shown with grey, blue, and red traces, respectively.  $^{13}\text{C}$  labelling as shown in Figure 12,  $n = 6$ . The dashed red lines indicate transitions between different solid forms.

Polarization solid-state NMR data in Figure 16 gives information on structure and dynamics of  $\alpha$ -CD in the solid state. The DP(grey) spectra gives qualitative information in the CD molecule while the CP(grey) gives information about more rigid segments of the CD molecule. INEPT(red) indicates more mobile segments in the CD molecule. The lack of INEPT signal is a strong indication that the CD molecules can be regarded as rigid. PTssNMR can be used as a "fingerprint" to easily identify solid-solid phase transitions. For the dry form of  $\alpha$ -CD, the PTssNMR data reveal a phase transition between two polymorphs between 65 and 75 °C. For  $\alpha$ -CD equilibrated at 6% RH, on the other hand, the transition to the high-temperature polymorph occurs between 35 and 45 °C. From this, we conclude that the thermal behaviour of CD polymorphs is extremely sensitive to water activity.

## $\beta$ -CD

X-ray diffractograms of  $\beta$ -CD at different water activities are shown in Figure 17. A solid-solid transition occurs at a water activity of 11.3-21.6 %RH which is lower than for  $\alpha$ -CD and with the PXRD showing a less dramatic change.

The water adsorption isotherm of  $\beta$ -CD in Figure 14 show three distinct regimes: one initial regime at low water activity, an intermediate regime, and a regime at a water activity above 30 %RH. At low water activity the increase with respect to water activity is small. In the intermediate regime there is a dramatic change in the isotherm due to a re-crystallisation which is in agreement with PXRD data indicating a solid-state structure transition. At high water activity, the adsorption isotherm reaches a saturation level at 11 waters per CD molecule. The TGA data on the fully hydrated form is in agreement with this level of hydration, see Figure 19. It agrees with the  $\beta$ CD-9H<sub>2</sub>O previously reported by Damodharan et al.[72–74, 80]

PTssNMR on  $\beta$ -CD in the temperature range 5-75 °C in Figure 20 indicate that the <sup>13</sup>C segments in the solid  $\beta$ -CD hydrates are rigid. Only CP (blue) signal intensity is present. No temperature-induced polymorphic transitions are observed. However, the polymorph after equilibrating at 6 %RH, and the one obtained at 53 %RH are easier to distinguish with the PTssNMR than PXRD.

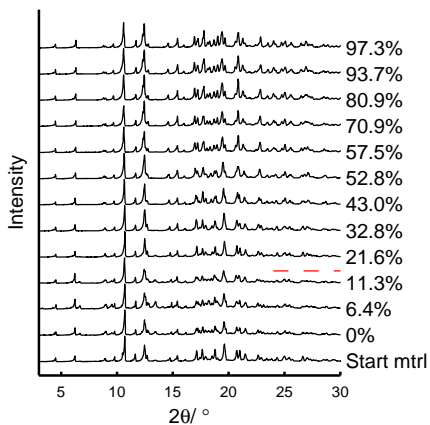


**Figure 17:** X-ray diffractograms at ambient temperature of  $\beta$ -CD starting material and equilibrated at increasing water activity in units of relative humidity. The dashed red line indicates a solid-state transition.

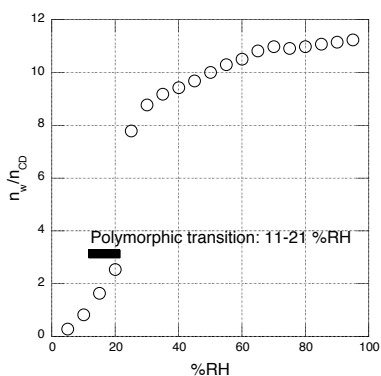


**Figure 18:** GVS data on  $\beta$ -CD, given as the number of water molecules per CD molecule, as a function of relative humidity. The bar indicates the solid-state transition region indicated in the PXRD data in Figure 17.

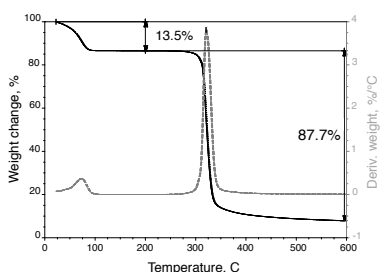


**Figure 19:** TGA data on  $\beta$ -CD equilibrated at 11.3% RH (LiCl). The initial mass loss of 13.5% corresponds to 9.80 water molecules per CD molecule.

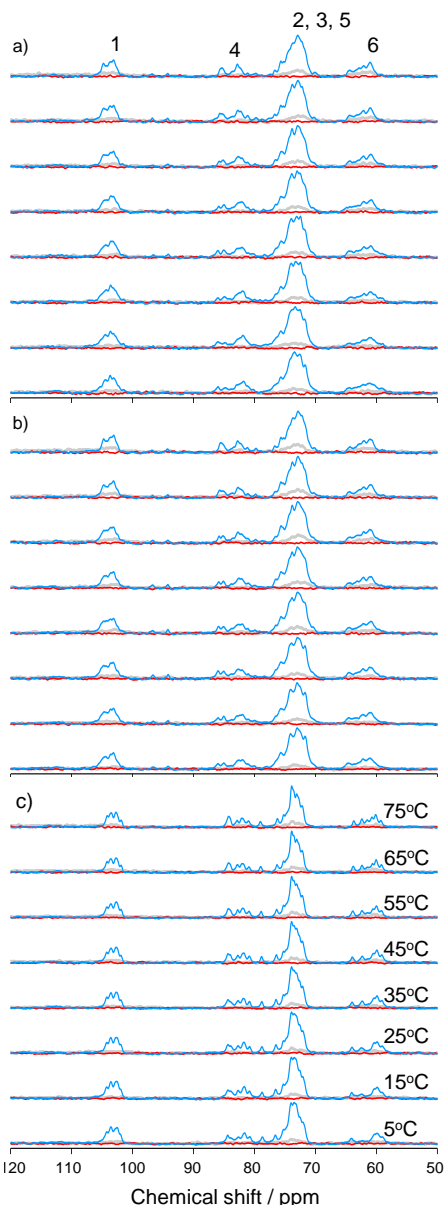


**Figure 20:** Solid-state  $^{13}\text{C}$  PTsNMR spectra of  $\beta$ -CD at different temperatures equilibrated under dry conditions (a) and at 6%RH (b). Spectra acquired at  $B_0=11.74$  T with 5 kHz magic-angle spinning and 68 kHz TPPM  $^1\text{H}$  decoupling. DP, CP, and INEPT spectra are shown with gray, blue, and red traces, respectively.  $^{13}\text{C}$  labelling as shown in Figure 12,  $n = 7$ .

## $\gamma$ -CD

$\gamma$ -CD shows two solid-state transitions in the water activity range 0-97.3 %RH, see Figure 21. The first transition occurs in the same RH range (11.3-21.6 %RH) as for  $\beta$ -CD, and again only with small changes in the structure according to the PXRD.

The GVS data show the same trend as for the  $\beta$ -CD case, see Figure 23. In the low humidity range 5 water molecules are absorbed. At the water activity range 52.8-57.5 %RH, X-ray data indicate a structural change. The X-ray diffractogram for  $\gamma$ -CD equilibrated at 57.5 %RH shows clear evidence of substantial amorphisation as a (presumably) transient part of the structural rearrangement. The number of water molecules per CD increases from 7 to 15 in this transition. At even higher water activity 97.3 %RH ( $K_2SO_4$ ), the isotherm levels off at around 16 water molecules per CD molecule. This is in agreement with the TGA data presented in Figure 23 and with the  $\gamma$ CD-14H<sub>2</sub>O previously reported by Harata et al[34, 72-74].

<sup>13</sup>C PTssNMR spectra of the three different solid forms of  $\gamma$ -CD are presented in Figure 24. As previously observed for  $\alpha$ - and  $\beta$ -CD, no INEPT signal is present. Indicating that the molecular segments are rigid in the CD molecules, regardless of the level of hydration.

## Summary

The TGA for all three CD systems (Figures 15, 19 and 23) agree well with data reported for the fully hydrated CD forms. At water activities below full hydration the TGA data disagreed with the GVS data and the fully hydrated forms were obtained instead. The explanation for this must be sorption of water during sample loading. Also in experimental parameter setup in the GVS was so that re-crystallisation could occur. The GVS experiments with a duration of ca 12 hours is at least an order of magnitude faster than that of the equilibration prior to PXRD experiments (weeks). In GVS, PXRD and NMR data, there is more control over sample handling/preparation and data collection. The risk of unwanted water uptake is much lower. We are therefore confident that our CDs are crystalline in the solid state, and have no water molecules in their crystal lattice. To the best of our knowledge, this is first time evidence for crystalline anhydrides of cyclodextrins.

The GVS data reveal that the moisture uptake at low water activity is size dependent and that the solid forms are stable. The adsorption isotherms for all the CDs is roughly linear in the beginning, but with different slopes (Figures 14, 18 and 22) At 15 %RH, the  $\alpha$ -,  $\beta$ - and  $\gamma$ -CD have adsorbed 4.0, 1.6 and 2.2 water molecules per CD, respectively.

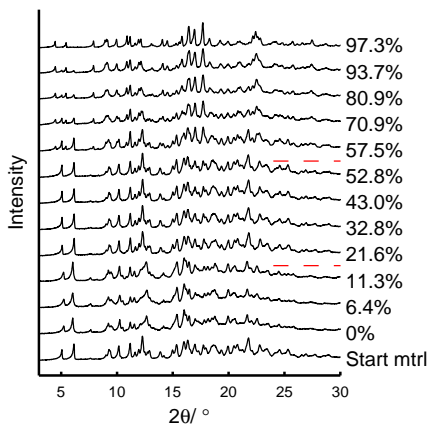


**Figure 21:** X-ray diffractograms at ambient temperature of  $\gamma$ -CD starting material and equilibrated at increasing water activity in units of relative humidity. The dashed red line indicates a solid-state transition.

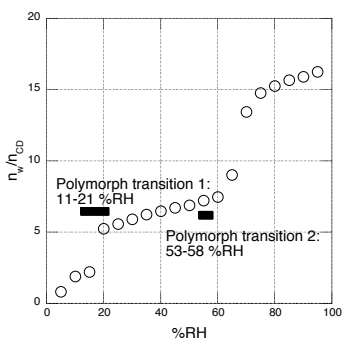


**Figure 22:** GVS data on  $\gamma$ -CD, given as the number of water molecules per CD molecule, as a function of relative humidity. The bar indicates the solid-state transition region indicated in the PXRD data in Figure 13.

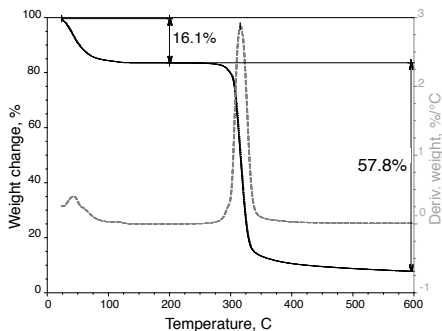


**Figure 23:** TGA data on  $\gamma$ -CD equilibrated at 97.3 %RH ( $K_2SO_4$ ). The initial mass loss of 16.1 % corresponds to 13.8 water molecules per CD molecule.

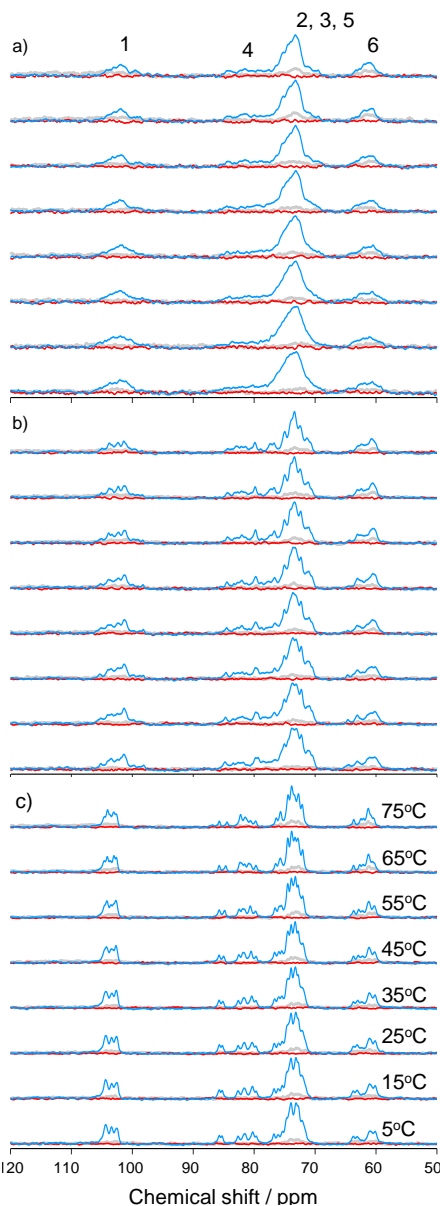


**Figure 24:** Solid-state  $^{13}C$  PTssNMR spectra of  $\gamma$ -CD at different temperatures equilibrated under dry conditions (a) and at 6 %RH (b). Spectra acquired at  $B_0=11.74$  T with 5 kHz magic-angle spinning and 68 kHz TPPM  $^1H$  decoupling. DP, CP, and INEPT spectra are shown with gray, blue, and red traces, respectively.  $^{13}C$  labelling as shown in Figure 12,  $n = 8$ .

This implies that the anhydrous  $\alpha$ -CD should be considered to be more hydrophilic than the anhydrates of  $\beta$ -CD and  $\gamma$ -CD. Also, the adsorption isotherm for  $\alpha$ -CD differs from that of  $\beta$ -CD and  $\gamma$ -CD in that during the structural transition to another polymorph the slope of the isotherm decreases. The opposite occurs in the adsorption isotherms of  $\beta$ - and  $\gamma$ -CD.

In the  $\alpha$ -case, the inflection point in the adsorption isotherm occurs after adsorbing 4 water molecules per CD molecule. One hypothesis is that this corresponds to the amount of water that can be accommodated in the CD cavity. Further water uptake induces a structural change as a way to be able to host additional water molecules in interstices in the crystal lattice. This hypothesis is not applicable on the case  $\beta$ - and  $\gamma$ -CDs. Their polymorphic transitions start at water contents far below the amount of water that could be accommodated in the CD cavity. For  $\beta$ - and  $\gamma$ -CDs cases, it could be hypothesised that the water occupies positions on the outside of the CD cavity first. Here they would induce a polymorphic transition primarily so the CD structure can accommodate water molecules in the cavity interior. However, this is not in agreement with the  $\alpha$ -case. This suggests that the driving forces behind the water-induced structural changes are probably not directly related to the amount of water that can be accommodated in the CD structure.

The PTssNMR is a good complement to the PXRD to determine structures. The PTss-NMR data indicated a solid-like “rigid” character of all the moieties in the CDs carbohydrate backbone. Surprisingly, it was affected by neither temperature nor hydration level. The data does not support that the CDs structures should be regarded as dynamic. Only close to the actual phase transition where the structural re-arrangement occurs.

## Paper III Polarization transfer solid-state NMR: a new method for studying cellulose dissolution

In paper III we used Polarization Transfer solid state Nuclear Magnetic Resonance (PTssNMR) techniques[10, 60], for a detailed molecular characterization of partially dissolved cellulose, i.e. the dissolution medium with co-existence between solid and dissolved cellulose. As discussed in the introduction, the PTssNMR  $^{13}\text{C}$  chemical shifts gives information about molecular structure, conformation, and packing and the signal intensities from the CP[61] and INEPT[62] gives information about molecular dynamics.

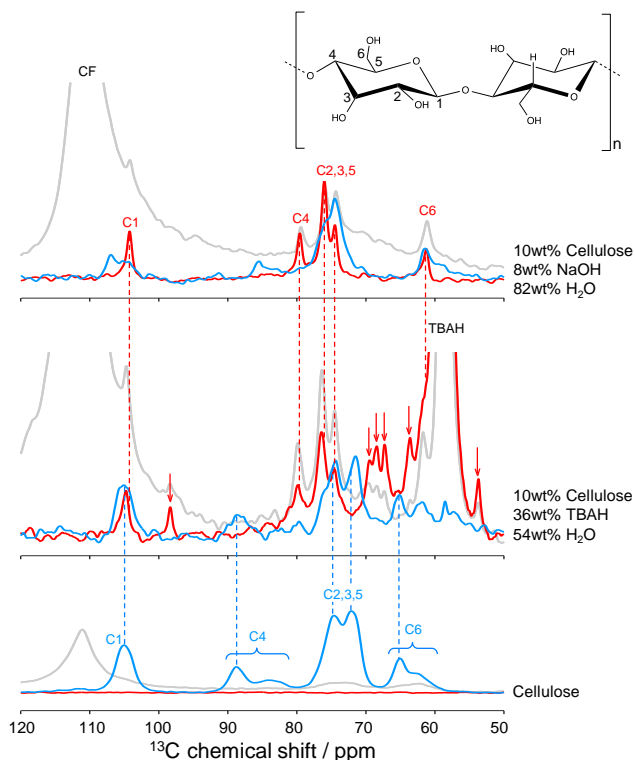


**Figure 25:** PTssNMR spectra of the starting material dry microcrystalline cellulose I (bottom), partially dissolved in aqueous TBAH (middle), and dissolved in NaOH (top). The DP (grey) spectra can be seen as a reference. The CP (blue) and INEPT (red) spectra can be seen as solid and dissolved cellulose peaks, respectively.  $^{13}\text{C}$  assignment is described in the structure formula of the cellulose repeat unit. The blue and red dashed lines represent literature data for cellulose I in wood pulp fibers[81] and dissolved cellulose.[82] respectively. The TBAH peak is from the  $\text{TBA}^+$  ions and the CF peak originates from the Teflon spacer of the MAS rotor. The red arrows indicate  $\text{TBA}^+$  breakdown products. The spectra was acquired at 25 °C and 125 MHz  $^{13}\text{C}$  Larmor frequency with 5 kHz MAS and 88 kHz TPPM  $^1\text{H}$  decoupling. Only the relevant spectral range is depicted here and the spectra have been magnified to facilitate the viewing of the cellulose resonance lines.

In Figure 25 are  $^{13}\text{C}$  PTsNMR spectra of cellulose at various stages of dissolution. The  $^{13}\text{C}$  chemical shifts of the cellulose peaks are compiled in Table 1. As discussed previously, the CP (blue) and INEPT (red) spectra visualises which segments that have slow (CP) or fast (INEPT) molecular dynamics. The DP (grey) spectra is only included as a reference. The bottom spectra on the dry cellulose yields intense CP peaks. As expected, for solid cellulose, the INEPT signal is absent. The observed CP  $^{13}\text{C}$  chemical shifts agree with previously reported data on cellulose I,[40, 83]. The shifts at 105.4 (C1), 89.1 (C4), 75.3/72.7 (C2,3,5), and 65.5 ppm (C6) agree particularly well with data reported for wood pulp fibers[81] with low crystallinity.

The middle spectra represents cellulose dissolved in aqueous tetrabutylammonium hydroxide (TBAH). Both CP and INEPT signal is observed in the spectra indicating that solid and liquid/dissolved components are present in the system. Several of the observed CP peaks are in good agreement with the ones found for the starting material of dry cellulose I (indicated with blue dotted lines), indicates that there is still undissolved residues of cellulose I in the system. There are a multitude of INEPT peaks. The main INEPT peak originates from the  $\text{TBA}^+$  ions four inequivalent carbons. Only one of them is in view in the ppm range depicted here in Figure 25. The INEPT peaks assigned to dissolved cellulose are indicated with red dotted lines. The chemical shifts agree with literature data reported for ultra-centrifuged samples of regenerated cellulose dissolved in 10 wt% NaOH(aq): 104.7 (C1), 79.9 (C4), 76.4/75.0 (C2,3,5), and 61.9 (C6) ppm.[82] The theoretical intensity calculations for the PTsNMR techniques[10, 60] for cellulose implies that the CH-bonds in the molecule reorient on a time-scale faster than 100 ns. This is a strong indication that the cellulose is indeed molecularly dissolved. Deconvolution calculations on the DP peaks from dissolved cellulose,  $\text{TBA}^+$ , and tributylamine yields a fraction of  $\text{TBA}^+$  breakdown of approximately 4.9 % and a molar ratio between the tributylamine and the glucose units of the dissolved cellulose of approximately 11 %. The remaining INEPT peaks are assigned to tributylamine and 1-butene which are formed from the  $\text{TBA}^+$  ions by Hofmann elimination.[84]

**Table 1:** Chemical shifts of partially dissolved cellulose<sup>a</sup>

Sample	Fraction	Carbon atom				Comment
		C1	C4	C 2, 3, 5	C6	
Dry	Solid	105.1	88.8	74.6, 72.1	65.0	Cellulose I
TBAH	Solid	105.1	88.7	74.4, 71.5	65.1	Cellulose I
	Dissolved	104.7	79.8	76.4, 74.5	61.7	
NaOH	Solid	107.1	85.6	75.8, 74.6	61.5	Cellulose II
	Dissolved	104.3	79.6	76.0, 74.5	61.3	

<sup>a</sup> Shifts calibrated with respect to  $\alpha$ -glycine at 176.03ppm as external standard with a precision of  $\pm 0.2$ ppm given by the acquisition time.

The top spectra represents the NaOH(aq) cellulose solution. Both CP and INEPT intensity signals are present in the spectra. The CP signals agree with chemical shifts reported for cellulose II or regenerated cellulose.[40, 85] No chemical shifts agree with the ones observed for the starting material cellulose I. Hence, all the original cellulose I has been dissolved and that some of it has then precipitated out as cellulose II. The INEPT peaks are similar to the chemical shifts for the dissolved cellulose in the TBAH(aq) sample.

In conclusion, PTssNMR can be used to detect/investigate both solid and the dissolved cellulose in different steps of the dissolution process. The results presented here have been the basis for future studies of the mechanisms of cellulose dissolution with PTssNMR.[69]

## Paper IV Structure-Property Correlations of Ion-Containing Polymers for Fuel Cell Applications

In paper IV the self diffusion of water was investigated in ETFE-g-PSSA membranes with different grafting levels. The crosslinked membranes with a fixed grafting level of 25%, and a varying crosslinking level (corresponding to 0, 10 and 20 vol% (with respect to total monomer) of DiPB in the grafting solution). The self diffusion of water was investigated as a function of temperature and relative humidity.

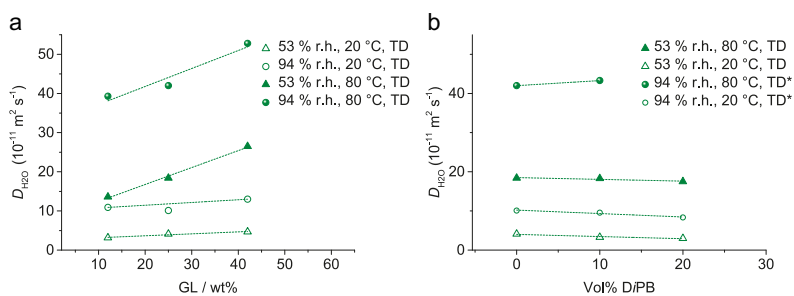


**Figure 26:** Diffusion coefficients of water in the systems a) ETFE-g-PSSA for different GL and b) ETFE-g-P(SSA-co-DiPB) at a fixed GL of 25 % and various crosslinking content.

At low temperature, 20 °C, the grafting level of the membranes have little influence on the self diffusion coefficient of water ( $D_{H_2O}$ ) in the membranes, see Figure 26a. However, at higher temperature, 80 °C, there is a significant change. Comparing with the self diffusion of pure water  $2.2 \cdot 10^{-9} \text{ m}^2 \text{ s}^{-1}$  at 21 °C and  $6.0 \cdot 10^{-9} \text{ m}^2 \text{ s}^{-1}$  at 80 °C[86]. The apparent water diffusion activation energy was estimated to be between 18-25 kJ/mol through the Arrhenius equation. The relative humidity (RH) and the temperatures affect the conductivity of the membranes more than the level of grafting.

The effect of the anisotropy of the base material on the diffusion coefficient by was analysed in ETFE-g-P(SSA-co-DiPB) membranes with a GL of 25 % with a crosslinking content of 10 vol% (wrt. total monomer). In the transverse direction (TD) the diffusion coefficient appears to be 1.5 times higher than in the machining direction (MD). (TD:  $1.83 \cdot 10^{-10} \text{ m}^2 \text{ s}^{-1}$ ; MD:  $1.21 \cdot 10^{-10} \text{ m}^2 \text{ s}^{-1}$ ). The transport property or water mobility in the membrane is not superior in MD to TD. Intuitively it should be the other way around considering that the base polymer chains are preferentially oriented in MD.

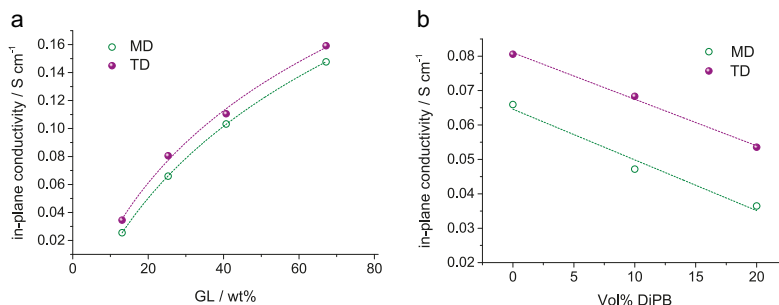


**Figure 27:** Conductivity of liquid water swollen membranes for MD and TD at 25 °C. a) ETFE-g-PSSA membranes with different grafting levels. b) ETFE-g-P(SSA-co-DiPB) membranes with different crosslinking levels at a fixed GL of 25 %.

In-plane proton conductivity agree with the diffusometry measurements on the importance of the anisotropy of the base film. Regarding properties associated with the grafted polymer TD is favoured over MD. At lower GL, the relative difference of MD and TD is up to 30 %. Upon increased GL this difference decreases, see Figure 27a. For a GL of 67 % this difference is still about 8 %. A high GL does not result in a completely uniform proton transport. For a crosslinked system with the same GL, the observed difference in MD and TD is even more pronounced, reaching almost 40 %, see Figure 27b.

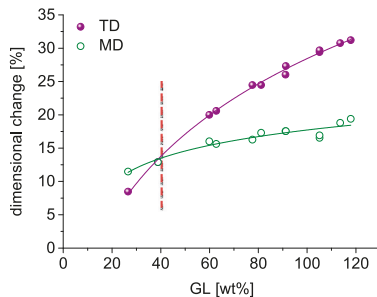


**Figure 28:** Dimensional change upon grafting for MD and TD of an ETFE film.

The dimensional change of the base film upon grafting was investigated on a macroscopic length scale. When a new polymer is grafted to the base polymer film it the base “swells” and becomes diluted. The dimensional change in TD and MD as a function of GL can be seen if Figure (28). Two different regimes are suggested. At low GL, the growth in MD is higher than in TD. At higher GL this changes and MD growth reaches what looks like a saturation level. Growth in TD continues to increase.

In all the techniques used in this study, TD stands out on the importance of anisotropy. The structure of the polymer film after fabrication is expected to be similar to TD. Regarding the function of the polymer membrane in the fuel cell this could be an advantage.

## 4 Conclusions

PTssNMR is a powerful technique that can be used as a complement to the more conventional solid state techniques used in characterizing solid, semi-solid, liquid phases, and co-existence regions of both natural and synthetic materials at low water contents. It provides information on molecular structure and dynamics (Papers I,II, and III). In paper I the equilibrium phase diagram of the  $C_{14}G_2/H_2O$  system was determined at low water contents and the regions of metastability of the non-equilibrium phases was reported. A new crystalline phase, the dihydrate (DH), was reported. In paper II the influence of water activity on the stability of crystalline hydrates of  $\alpha$ -,  $\beta$ -, and  $\gamma$ -cyclodextrin was determined. It was found that  $\gamma$ -CD crystallizes in three distinct structures and  $\alpha$ - and  $\beta$ -CD both crystallized in two different structures in the range 0-97.3 %RH.

In paper III we showed how PTssNMR can be used to investigate and estimate fractions of the solid and the dissolved cellulose components in aqueous dissolution medium. The molecular conformation and the molecular interactions can be followed through the chemical shifts. Also impurities can be detected. When considering the importance of hydrophobic interactions in the cellulose systems,[45] it is important to account for the effects from possible hydrophobic or amphiphilic co-solutes.

In paper IV we reported on the use of pulsed field gradient diffusion NMR to follow water diffusion in polymer electrolyte membranes with respect to grafting level, temperature, hydration level and anisotropy. In the transverse direction (TD) the diffusion coefficient appears to be 1.5 times higher than in the machining direction (MD). The grafting level of the membranes have little influence on the self diffusion coefficient of water at low temperatures. However, at higher temperature there is a significant change. The relative humidity (RH) and the temperatures affect the conductivity of the membranes more than the level of grafting does.

## 5 Acknowledgements

First of all I would like to thank my supervisors Daniel Topgaard, Stefan Ulvenlund and Johan Reimer for the opportunity to come to the physical chemistry department and perform this thesis work.

To all my coauthors, thank you for generously sharing your knowledge and expertise.

I would like to thank Jenny, Agnieszka, Tiago, Dat, Stephanie, Lennart, Göran and Christopher for all the help relating to NMR. Sven Lidin and Carola for all the help with the PXRD and Carlos and Annika for all the help with the TGA.

Special thanks to Ingegerd, Lennart, Majlis, Christopher, Maria, Ingrid and Helena for making all the practical details run smooth.

To everyone at the Physical Chemistry department, I would like to express my thanks for making my stay there so enjoyable. I have met so many strong and inspiring people and I am proud to call you my friends and colleagues.

I want to thank my study-group during my years as a graduate student. Especially Tommy G who has been a fellow traveller since day one (except for your brief stray to industry). Thank you for letting me tag along that first day to Kemicentrum and see what they had to offer.

Thursdays will forever be special in my heart Charlotte, Linnea, Magnus, and Aleksandra.

To Ingrid and Ronny thank you for all the help and support and for welcoming me into your family.

To mom, dad, Rebecka, Urban and Gabriel I would like to thank you for your support during these years in Lund and long before that. I appreciate all you have done for me and always tried to help smooth the way in any way you could.

To the love of my life Palle. You mean the world to me. Thank you for all the love and support during these years. You have been there since day one. To the biggest joy in my life, my son Alexander. You put a huge smile on my face every day. You have given me a new look on life and I love you to the moon and back my little one.

## 6 References

- [1] H. Kiwada, H. Niimura, Y. Fujisaki, S. Yamada and Y. Kato, *Chem. Pharm. Bull.*, 1985, **33**, 753–759.
- [2] F. A. Hughes and B. W. Lew, *J. Am. Oil Chem. Soc.*, 1970, **47**, 162–167.
- [3] S. Matsumura, K. Imai, S. Yoshikawa, K. Kawada and T. Uchibori, *J. Am. Oil Chem. Soc.*, 1990, **67**, 996–1001.
- [4] C. Baron and T. Thompson, *Biochim. Biophys. Acta*, 1975, **382**, 276–285.
- [5] F. Fischer and B. Helferich, *Liebigs Ann. Chem.*, 1911, 68–91.
- [6] G. A. Jeffrey and S. Bhattacharjee, *Carbohydr. Res.*, 1983, **115**, 53–58.
- [7] D. Balzer and H. Lüders, *Nonionic Surfactants*, Marcel Dekker, Inc., New York, 2000.
- [8] C. a. Ericsson, L. C. Ericsson, V. Kocherbitov, O. Söderman and S. Ulvenlund, *Phys. Chem. Chem. Phys.*, 2005, **7**, 2970–2977.
- [9] V. Kocherbitov and O. Söderman, *Langmuir*, 2004, **20**, 3056–3061.
- [10] A. Nowacka, N. A. Bongartz, O. H. S. Ollila, T. Nylander and D. Topgaard, *J. Magn. Reson.*, 2013, **230**, 165–175.
- [11] J. Szejtli, *Chem. Rev.*, 1998, **98**, 1743–1753.
- [12] W. Saenger, K. Gessler, T. Steiner, D. Hoffmann, H. Sanbe, K. Koizumi, S. M. Smith and T. Takaha, *Chem. Rev.*, 1998, **98**, 1787–1802.
- [13] K. A. Connors, *Chem. Rev.*, 1997, **97**, 1325–1357.
- [14] E. M. M. Del Valle, *Progress Biochemistry*, 2004, **39**, 1033–1046.
- [15] M. E. Brewster and T. Loftsson, *Adv. drug deliver. rev.*, 2007, **59**, 645–666.
- [16] L. Szente, J. Szejtli and G. L. Kis, *J. Pharm. Sci.*, 1998, **87**, 778–781.
- [17] T. Loftsson, M. Másson and M. E. Brewster, *J. Pharm. Sci.*, 2004, **93**, 1091–1099.
- [18] D. French, M. L. Levine, J. H. Pazur and E. Norberg, *Am. Chem. Soc.*, 1949, **71**, 353–356.
- [19] M. J. Jozwiakowski and K. A. Connors, *Carbohydr. Res.*, 1985, **143**, 51–59.

- [20] E. Sabadini and T. Cosgrove, *Carbohydr. Res.*, 2006, **341**, 270–274.
- [21] A. W. Coleman, I. Nicolis, N. Keller and J. P. Dalbiez, *J. Inclusion Phenom. Mol. Recognit. Chem.*, 1992, **13**, 139–143.
- [22] K. J. Naidoo, J. Y.-j. Chen, J. L. M. Jansson, G. Widmalm and A. Maliniak, *J. Phys. Chem. B*, 2004, **108**, 4236–4238.
- [23] C. Betzel, W. Saenger, B. E. Hingerty and G. M. Browns, *J. Am. Chem. Soc.*, 1984, **106**, 7545–7557.
- [24] W. Cai, T. Sun, X. Shao and C. Chipot, *Phys. Chem. Chem. Phys.*, 2008, **10**, 3236–3243.
- [25] G. Raffaini and F. Ganazzoli, *Chem. Phys.*, 2007, **333**, 128–134.
- [26] C. C. Rusa, T. A. Bullions, J. Fox, F. E. Porbeni, X. Wang, A. E. Tonelli, N. Carolina and N. Carolina, *Langmuir*, 2002, **18**, 10016–10023.
- [27] M. A. Hunt, C. C. Rusa, A. E. Tonelli and C. M. Balik, *Carbohydr. Res.*, 2004, **339**, 2805–2810.
- [28] M. A. Hunt, C. C. Rusa, E. Tonelli and C. M. Balik, *Carbohydr. Res.*, 2005, **340**, 1631–1637.
- [29] J. A. Ripmeester, *Supramol. Chem.*, 1993, **2**, 89–91.
- [30] T. Steiner and G. Koellner, *J. Am. Chem. Soc.*, 1994, **116**, 5122–5128.
- [31] B. Klar, B. Hingerty and W. Saenger, *Acta Crystallogr., Sect. B: Struct. Sci*, 1980, **36**, 1154–1165.
- [32] R. Puliti, C. Andrea Mattia and L. Paduano, *Carbohydr. Res.*, 1998, **310**, 1–8.
- [33] K. Lindner and W. Saenger, *Carbohydr. Res.*, 1982, **99**, 103–115.
- [34] K. Harata, *Bull. Chem. Soc. Jpn.*, 1987, **60**, 2763–2767.
- [35] J. M. MacLennan and J. J. Stezowski, *Biochem. Biophys. Res. Commun.*, 1980, **92**, 926–932.
- [36] K. Harata, *Chem. Lett.*, 1984, 641–644.
- [37] Y. Nakai, K. Yamamoto, K. Terada, A. Kajiyama and I. Sasaki, *Chem. Pharm. Bull.*, 1986, **34**, 2178–2182.
- [38] T. Uyar, M. A. Hunt, H. S. Gracz and A. E. Tonelli, *Crystal Growth & Design*, 2006, **6**, 1113–1119.

- [39] S. J. Kitchin and T. K. Halstead, *Solid State Nucl. Magn. Reson.*, 1996, 7, 27–44.
- [40] D. L. Vanderhart and R. H. Atalla, *Macromolecules*, 1984, 17, 1465–1472.
- [41] R. H. Atalla and D. L. Vanderhart, *Solid State Nucl. Magn. Reson.*, 1999, 15, 1–19.
- [42] A. C. O. Sullivan, *Cellulose*, 1997, 4, 173–207.
- [43] F. J. Kolpak and J. Blackwell, *Macromolecules*, 1976, 9, 273–27.
- [44] F. J. Kolpak and J. Blackwell, *Polymer*, 1978, 19, 132–135.
- [45] B. Lindman, G. Karlström and L. Stigsson, *J. Mol. Liq.*, 2010, 156, 76–81.
- [46] R. Bodvik, A. Dedinaite, L. Karlson, M. Bergström, P. Bäverbäck, J. Skov Pedersen, K. Edwards, G. Karlsson, I. Varga and P. M. Claesson, *Colloids Surf., A*, 2010, 354, 162–171.
- [47] R. P. Swatloski, S. K. Spear, J. D. Holbrey and R. D. Rogers, *J. Am. Chem. Soc.*, 2002, 124, 4974–4975.
- [48] S. Balog, U. Gasser, K. Mortensen, H. Ben, L. Gubler and G. G. Scherer, *J. Membr. Sci.*, 2011, 383, 50–59.
- [49] H. Ben, L. Gubler, A. Foelske-schmitz and G. G. Scherer, *J. Membr. Sci.*, 2011, 381, 102–109.
- [50] H. Ben, S. A. Gürsel, A. Buisson, L. Gubler, A. Wokaun and G. G. Scherer, *Fuel Cells*, 2010, 401–410.
- [51] D. S. A. D. Focatiis and L. Gubler, *Polym. Test.*, 2013, 32, 1423–1435.
- [52] M. A. Hickner, H. Ghassemi, Y. S. Kim, B. R. Einsla and J. E. Mcgrath, *Chem. Rev.*, 2004, 104, 4587–4612.
- [53] M. Rikukawa and K. Sanui, *Prog. Polym. Sci.*, 2000, 25, 1463–1502.
- [54] P. Jannasch, *Curr. Opin. Colloid Interface Sci.*, 2003, 8, 96–102.
- [55] V. Saarinen, K. D. Kreuer, M. Schuster, R. Merkle and J. Maier, *Solid State Ionics*, 2007, 178, 533–537.
- [56] S. J. Hamrock and M. A. Yandrasits, *J. Macromol. Sci., Part C*, 2006, 1797, year.
- [57] E. M. W. Tsang, Z. Zhang, Z. Shi, T. Soboleva and S. Holdcroft, *J. Am. Chem. Soc. Commun.*, 2007, 129, 15106–15107.
- [58] H. Nyqvist, *Int. J. Pharm. Tech. & Prod. Mfr.*, 1983, 4, 47–48.

- [59] J. Keeler, in *Understanding NMR Spectroscopy*, Wiley, 2005.
- [60] A. Nowacka, P. C. Mohr, J. Norrman, R. W. Martin and D. Topgaard, *Langmuir*, 2010, **26**, 16848–16856.
- [61] A. Pines, M. G. Gibby and J. S. Waugh, *J. Chem. Phys.*, 1972, **56**, 1776–1777.
- [62] G. A. Morris and R. Freeman, *J. Am. Chem. Soc.*, 1979, **101**, 760–762.
- [63] A. Nowacka, L. Douezan, L. Wadsö, D. Topgaard and E. Sparr, *Soft Matter*, 2012, **8**, 1482–1491.
- [64] E. Hellstrand, A. Nowacka, D. Topgaard, S. Linse and E. Sparr, *PLOS ONE*, 2013, **8**, e77235–e77235.
- [65] S. Björklund, T. Ruzgas, A. Nowacka, I. Dahi, D. Topgaard, E. Sparr and J. Engblom, *Biophys. J.*, 2013, **104**, 2639–2650.
- [66] S. Björklund, A. Nowacka, J. A. Bouwstra, E. Sparr and D. Topgaard, *PLOS ONE*, 2013, **8**, e61889–e61889.
- [67] S. Björklund, J. M. Andersson, Q. D. Pham, A. Nowacka, D. Topgaard and E. Sparr, *Soft Matter*, 2014, **10**, 4535–4546.
- [68] S. Gustavsson, L. Alves, B. Lindman and D. Topgaard, *RSC Advances*, 2014, **4**, 31836–31839.
- [69] L. Alves, B. Medronho, D. Topgaard and B. Lindman, *Cellulose*, 2016, **23**, 247–258.
- [70] J. E. J. Tanner, *J. Chem. Phys.*, 1970, 2523–2526.
- [71] H. Kirsebom, *Macromolecules*, 2009, 5208–5214.
- [72] F. H. Allen, *Acta Crystallogr.*, 2002, **B58**, 380–388.
- [73] I. J. Bruno, J. C. Cole, P. R. Edgington, M. Kessler, C. F. Macrae, P. McCabe, J. Pearson and R. Taylor, *Acta Crystallogr.*, 2002, **B58**, 389–397.
- [74] C. F. Macrae, P. R. Edgington, P. McCabe, E. Pidcock, G. P. Shields, R. Taylor, M. Towler and J. van de Streek, *J. Appl. Cryst.*, 2006, **39**, 453–457.
- [75] T. Instruments, *TGA Q500 Description*, 2016, <http://www.tainstruments.com/q500/>.
- [76] H. Sjögren, C. A. Ericsson, J. Evenäs and S. Ulvenlund, *Biophys. J.*, 2005, **89**, 4219–4233.

- [77] W. L. Earl and D. L. VanderHart, *Macromolecules*, 1979, **12**, 762–767.
- [78] H. Walderhaug, O. Söderman and P. Stilbs, *J. Phys. Chem.*, 1984, **88**, 1655–1662.
- [79] J. Seddon and R. Templer, in [*handbook of biological Physics*] *Structure and Dynamics of Membranes vol 1 - From Cells to Vesicles*, Elsevier, 1995.
- [80] L. Damodharan, V. Patabhi and N. K., *Mol. Cryst. Liq. Cryst.*, 2004, **423**, 17–35.
- [81] K. Kamide, K. Okajima, T. Matsui and K. Kowsaka, *Polym. J.*, 1985, **17**, 701–706.
- [82] K. Kamide, K. Okajima, T. Matsui and K. Kowsaka, *Polym. J.*, 1984, **16**, 857–866.
- [83] H. Kono, T. Erata and M. Takai, *Macromolecules*, 2003, **36**, 5131–5138.
- [84] in *Encyclopedia of Reagents for Organic Synthesis*, ed. E. L. Paquette, 2004.
- [85] H. Kono, Y. Numata, T. Erata and M. Takai, *Macromolecules*, 2004, **37**, 5310–5316.
- [86] T. Dippel and K. D. Kreuer, *Solid State Ionics*, 1991, **46**, 3–9.

